nature portfolio

# Peer Review File

# Lattice-Matched Molecular-Anchor Design for High-Performance Perovskite Quantum Dot Light-Emitting Diodes

Corresponding Author: Professor Dongxin Ma

**This file contains all reviewer reports in order by version, followed by all author rebuttals in order by version.**

Version 0:

Reviewer comments:

Reviewer #1

(Remarks to the Author)
In this work, Chen et al designed and synthesized a multi-anchor ligand TMeOPPO based on a widely-used ligand TPPO, which perfectly matches the lattice constant of CsPbI3 QDs. This ligand could coordinate with surface Pb2+ and provide effective passivation on surface defects. Based on the optimized QDs, high-performance QLEDs with a superior half-life of 23,000 h were achieved. The performances of both QDs and QLEDs are charming, while the most important part, the mechanism of the ligand, lacks a deeper exploration. Since various multiidentate ligands in perovskite QDs were proposed since 2018 (ACS Energy Lett. 2018, 3, 641-646, Nature,2024, 631,73–79) or even earlier, it was not so important to emphasize the benefits of multi-anchor ligands compared to single-anchor ligands. Indeed, the lattice-matched anchoring of surface ligands is an inspiring strategy and likely to be the main reason for achieving the remarkable performances in the work. I suggest that the authors discuss the lattice-match part more to make the work more inspiring for readers. The following concerns should also be settled:
1. In Fig.2, we could only find that TMeOPPO can act as a surface ligand, while it is still not clear about the single-anchor or multi-anchor coordination, since a single-anchor ligand may also obtain similar results. Authors should provide relevant evidence (experimentally or theoretically) about the multi-anchor effect.
2. In Fig.5, what is the reason for the differences in the QLED performances based on TFPPO, TClPPO, and TBrPPO-treated QDs? The author should discuss the results. I also suggest that authors present three models: single-anchor, multi-anchor, and lattice-matched multi-anchor, to highlight the superiority of the strategy, instead of providing three single-anchor ligands.
3. In DFT results, why were the band gaps of the three models all larger than 2.3 eV, since they simulate the band structure of CsPbI3 QDs?
4. The air-processed QLEDs based on target QDs could achieve a comparable EQE value with as-fabricated QLEDs. What is the reason for this phenomenon? Can all well-passivated QDs achieve high-performance QLEDs in air? Or is it attributed to the unique properties of TMeOPPO?
5. Why is the surface ligand density of target QDs lower (line 157) than control QDs? Since TMeOPPO shows stronger coordination with surface Pb2+, it seems they are more tightly bound to the surface and harder to be washed than OA/OAm during purification.
6. Why are the hole trap densities of both control and target QDs so high, about 1018 cm-3, even three-order higher than other reported CsPbI3 QDs?
7. The J-V curve of the control QLED looks abnormal. The authors also mentioned that the target QLEDs yield a 3-fold radiance of the control device at 6.8 V (line 183), but the current density of Target QLEDs at 6.8 V is 5 times larger than that of control QLEDs (Fig.4d). This result seems inconsistent with the EQE curves.
8. Fig.5c has not summarized a recent reported high-performance QLEDs (Sci. Adv. 2025, 11, eads7159).

Reviewer #2

(Remarks to the Author)
In this work, Chen et al. designed a new molecule according to the lattice characteristics of perovskite quantum dots. The lattice-matched molecular anchor enables QLED with a high EQE of 27% and excellent stability under operation, high current density and water-oxygen environment. Overall, this work could useful to the broad community working on optoelectronic properties of perovskites and inspire researchers to design molecules on demand. I am supportive of

publication in Nature Communications after addressing following concerns.
1. The authors chose TPPO as the basic molecular framework, and I noticed that TPPO should also have an enhancing effect on the performance of the device theoretically. Please conduct the TPPO-treated QLEDs.
2. I am very interested in the EQE changes of the air-processed QLED after being stored for some time. Please provide relevant experiments to verify the storage stability of air-processed QLED, as well as detailed preparation conditions for the air-processed QLED, especially the air humidity.
3. In Figures 2f and g, the 1H NMR spectra of the target QDs showed a higher chemical shift, while the 31P NMR spectra of the target QDs showed a lower chemical shift. Please provide a detailed explanation.
4. Please provide the fitting details (bi-exponential or tri-exponential equation) for TRPL measurements.
5. Could the molecular anchor stabilize octahedrons and maintain lattice stability, thereby inhibiting ionic migration?
6. The descriptions of the type of ligands should be checked carefully. For example, does the halogen in TFPPO participate in passivation? If so, the ligand type description in the manuscript and Table 1 should be carefully reviewed. If not, a clear rationale for comparing the lengths of different groups in the F-substituted ligand is required. Other ligands are the same as TFPPO.
7. The labelled number in Fig.S2 is misleading, please check it.

Reviewer #3

(Remarks to the Author)
This study by Zhang and coauthors compare a series of organic molecules, TPPO, TMeOPPO, TFPPO, TClPPO, TBrPPO that can anchor the defect sites in perovskite quantum dots. The authors conduct a series of film and LED device characterizations and conclude that the TMeOPPO offers the best performance among the series. The reason was claimed to be that the TMeOPPO can provide multisite defect anchoring since the distance between the oxygen atoms of the P=O group and the –OCH3 group is 6.5 Å, which matches perfectly with the lattice spacing of CsPbI3 quantum dots (also 6.5 Å). Overall, this is one of the plethora of perovskite surface passivation studies where a good cause-strategy-impact is shown, but a new understanding to the field is much to be desired. While the trend is suggestive, I have a number of concerns including experimental data validation, data interpretation and display. These concerns make it unable for me to recommend publication in Nature Communications. I provide more detailed comments below:

(1) The authors pick a series of triphenylphosphine oxides with different substitution groups (-OCH3, -F, -Cl, -Br), and thus different interatomic distance (the authors' word) between the substitution group and the P=O group in the framework. However, there are other variables, primarily the interaction between the substitution groups with un-coordinated Pb2+. Clearly, the –OCH3 group has stronger passivation effects on perovskites than the rest of groups. If the trend is indeed due to the ability of a single molecule to anchor two sites due to perfectly-matched (both 6.5 Å) interatomic distance of the passivator with the lattice spacing of CsPbI3 perovskite, and not, for instance, due to the presence of optimal -OCH3 group, the authors will need to conduct reference experiments to rule it out. Overall, I feel that the authors need to compare more than a single series to validate their claim, rather than simply found a specific series where the –OCH3 substituted passivator work better.

(2) Here, the authors report improved "EQE of up to 27%" and "peak luminance of ~ 10^3 cd/cm2 (Fig. S5), and operating half-life of over 23000 h".

i. These improvements appear real vs an internal control. However, the device performance, particularly luminance, still remain clearly inferior to existing perovskite QLEDs reports in the literature as summarized in Xiong et al., Nature, 2024, 633, 344 – 350. Can the authors comment on this, and maybe consider/discuss mitigation strategies to address this? Meanwhile, can the authors plot EQE-Luminance for direct comparison?
ii. Since half lifetime of LED is dependent on the current density and the initial luminance, and considering that the long life-time is one main claim of this manuscript, to ensure fair and direct comparison, I would recommend the authors to either follow the suggested test protocols (both 100 and 1000 cd/m2) as suggested by Woo et al., Nat. Photon., 2021, 15, 630 – 634, or plot the half lifetime of fabricated LEDs against current density and compare that with the LED half lifetime summary by Zhao et al., Matter, 2024, 7, 772 – 793.
iii. Statistics are very important for comparing device performance, the authors should report statistics rather than single value, especially in Table 1.

(3) Overall, the manuscript would benefit from more discussion of the results, and what was learnt, rather than simply stating what the results were. As an example, in Figure 6, the authors simply introduced the radiance, EQE and T50 data of LEDs treated with TFPPO, TClPPO and TBrPPO, without discussing possible reasons causing the difference.

(4) In the energy level diagram shown in Figure 4c, the schematic appears to place the LUMO of PEDOT:PSS:PFI below –5.5 eV, and indicate that holes are injected from the ITO into the LUMO of PEDOT:PSS:PFI, which is conceptually incorrect and misleading. How do the authors determine the energy levels of PEDOT:PSS:PFI? If the authors intended to depict the work function instead of the LUMO/HOMO levels, the figure should be revised to reflect this distinction clearly.

(5) There are lots of discrepancies in the presented experimental data. For example, the authors report that in their QLED device, the PEDOT:PSS:PFI layer is 180 nm thick, the PTAA layer is 40 nm, the perovskite QD layer is 30 nm, and the TPBi layer is 40 nm. Several concerns arise from these claims:
i. What is the rationale for using an HTL with a total thickness of approximately 220 nm? Such a thick HTL is likely to introduce significant series resistance, potentially hindering hole injection efficiency.

ii. The reported film thicknesses are counterintuitive based on the stated fabrication conditions. Specifically, spin-coating PEDOT:PSS at 4000 rpm for 45 seconds would not typically yield a film as thick as 180 nm. Similarly, a 5 mg/mL PTAA solution spin-coated 4000 rpm for 45 seconds would not be expected to result in a 40 nm film. How were these thicknesses determined? The authors should provide measurement data to substantiate these values.
iii. The reported film thicknesses also appear inconsistent with the SEM cross-sectional image in Figure 4b. The scale bar is not labeled, making interpretation difficult; however, visually, the PTAA layer appears roughly three times thicker than the TPBi layer, despite both being reported as 40 nm. Moreover, PTAA also seems approximately three times thicker than the ITO layer, which is also not expected. These discrepancies raise concerns about the accuracy of the layer assignments in the SEM image.

(6) Missing critical experimental details: the manuscript omits lots of experimental details which are crucial for understanding the actions and ensuring reproducibility. For instance:
i. The authors simply stated “For the target QDs, TMePPO in ethyl acetate was added during the purification process”. What is the concentration of TMePPO solution? What is the volume ratio of TMePPO solution relative to the QD solution? Has the TMePPO replaced the ligands (OA, OAm)? This might explain the size changes in STEM images in Figure 2b? These information is vital for elucidating the role of TMePPO in surface treatment and should be clearly stated.
ii. The description of sample fabrication and characterization processes lacks important details. For instance, with regards to HTL, the authors simply wrote “a mixture of PEDOT: PSS and PFI solutions was spincoated onto ITO-coated glass substrates” without mentioning the concentration and choice of solvents; For air-processed QLEDs, the authors wrote “we spun PEDOT:PSS:PEI, PTAA and QD solution in the atmosphere” without mentioning important details such as humidity; For PL measurement, the excitation source, its wavelength and fluence are not mentioned.

Version 1:

Reviewer comments:

Reviewer #1

(Remarks to the Author)
The authors have adequately addressed the questions raised by this reviewer, and the overall data presentation has become more coherent, thereby strengthening the robustness of their claims. Therefore, the reviewer recommends the publication of this paper in Nature Communications.

Reviewer #2

(Remarks to the Author)
The author have addressed all my concerns. The revised manuscript is suitable for publishing

Reviewer #3

(Remarks to the Author)
The authors have adequately addressed most of my concerns.

We appreciate reviewers' helpful comments and have replied to them point by point in the following content. For clarity, reviewers' original comments and our responses are in blue font, and the changes we made to the main text are quoted in red font. We have also highlighted the corresponding modifications in the revised manuscript.

## Replies to Reviewer #1

**Comments to the Author:**

In this work, Chen et al designed and synthesised a multi-anchor ligand TMeOPPO based on a widely-used ligand TPPO, which perfectly matches the lattice constant of $CsPbI_3$ QDs. This ligand could coordinate with surface $Pb^{2+}$ and provide effective passivation on surface defects. Based on the optimised QDs, high-performance QLEDs with a superior half-life of 23,000 h were achieved. The performances of both QDs and QLEDs are charming, while the most important part, the mechanism of the ligand, lacks a deeper exploration. Since various multiidentate ligands in perovskite QDs were proposed since 2018 (ACS Energy Lett. 2018, 3, 641-646, Nature, 2024, 631,73-79) or even earlier, it was not so important to emphasise the benefits of multi-anchor ligands compared to single-anchor ligands. Indeed, the lattice-matched anchoring of surface ligands is an inspiring strategy and likely to be the main reason for achieving the remarkable performances in the work. I suggest that the authors discuss the lattice-match part more to make the work more inspiring for readers. The following concerns should also be settled.

**Comment 1:** In Fig.2, we could only find that TMeOPPO can act as a surface ligand, while it is still not clear about the single-anchor or multi-anchor coordination, since a single-anchor ligand may also obtain similar results. Authors should provide relevant evidence (experimentally or theoretically) about the multi-anchor effect.

**Response:** We have now provided both experimental and theoretical evidence about the multi-anchor effect.

(i) Experimental evidence

To study the difference between single-site and multi-site molecules, we have now synthesised TPPO-treated QDs and fabricated the corresponding QLED. The pristine, TPPO-treated, and TMeOPPO-*p*-treated

QDs showed average PLQYs of 59%, 70% and 96%, respectively. We have also demonstrated the performance and operating stability of the corresponding devices (**Fig. R1.1**). The QLED based on TPPO-treated QDs showed a maximum radiance of 49,018 mW $Sr^{-1}$ $m^{-2}$, a maximum EQE of 19.79% and a $T_{50}$ of 1,944 h. It can be concluded that QLED based on TPPO-treated QDs (single-site anchor) showed better EL performance and operating stability compared to the pristine device, but not as good as QLED based on TMeOPPO-*p*-treated QDs (multi-site anchor) (**Table R1.1**).

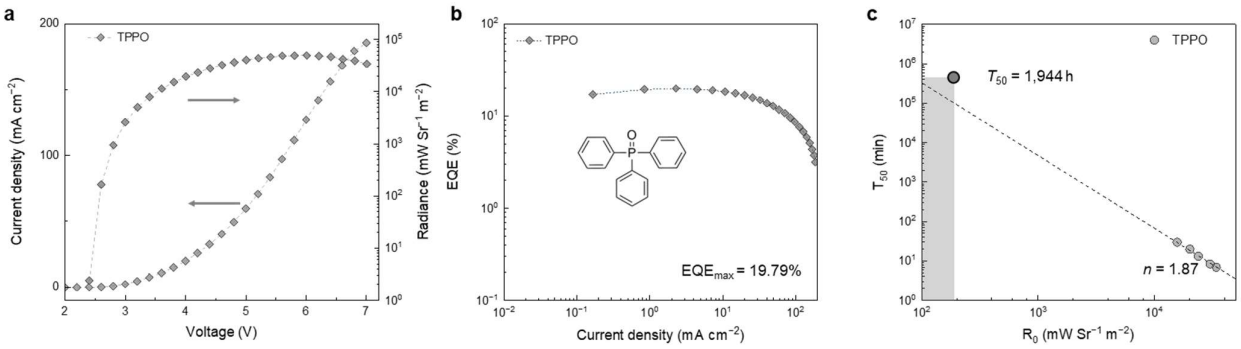


**Fig. R1.1** EL performance and stability of QLEDs based on TPPO-treated QDs. **a,** Current density-radiance-voltage curve. **b**, EQE curve (the insert is the chemical structure). **c**, Operating stability.

**Table R1.1** EL performance of QDs treated with different molecules

| **Device** | **Type** | **Radiance** (**mW $Sr^{-1}$ $m^{-2}$**) | **EQE$_{max}$** (**%**) | **EQE$_{average}$** (**%**) | **$T_{50}$*** (**h**) |
|---|---|---|---|---|---|
| Control | / | 42,809 @6.8 V | 15.14 | 12.8 | 1,350 |
| TPPO | Single-site | 49,018 @6.0 V | 19.79 | 17.7 | 1,944 |
| TMeOPPO-*p* | Multi-site | 119,037 @6.8 V | 26.91 | 25.3 | 23,420 |

*For initial radiance of 190 mW $sr^{-1}$ $m^{-2}$, equivalent to a luminance of 100 cd $m^{-2}$ for green perovskite LEDs.

(ii) Theoretical evidence

We have now added the electrostatic potential (ESP) of the single-site molecule TPPO and the projected density of states (PDOSs) of QDs treated with TPPO. We found that the P=O group exhibited strong nucleophilicity, allowing TPPO to offer a single-site interaction with uncoordinated $Pb^{2+}$ (**Fig. R1.2**). The PDOS results revealed that the Pb-6$p_z$ trap states around the Fermi level were completely eliminated by O-2*p*,

whereas the uncoordinated $Pb^{2+}$ maintained the trap states. Meanwhile, the trap peaks were separated from the conduction band minimum state, showing that the consecutive trap states could not be eliminated sufficiently (**Fig. R1.3b**). The P=O and -$OCH_3$ groups both have strong nucleophilicity, thus TMeOPPO-*p* can offer multi-site interaction. The PDOS results showed that the trap states and the CBM peaks were completely connected in TMeOPPO-*p*-treated QDs, indicating that TMeOPPO-*p* could strongly interact with uncoordinated $Pb^{2+}$, stabilise the lattice, and eliminate the trap states entirely (**Fig. R1.3c**).

According to the experimental and theoretical evidence presented above, we have reached the following conclusions: the single-site molecule could improve QD and device performance to some extent; however, its effect is far less significant than that of multi-site molecules.

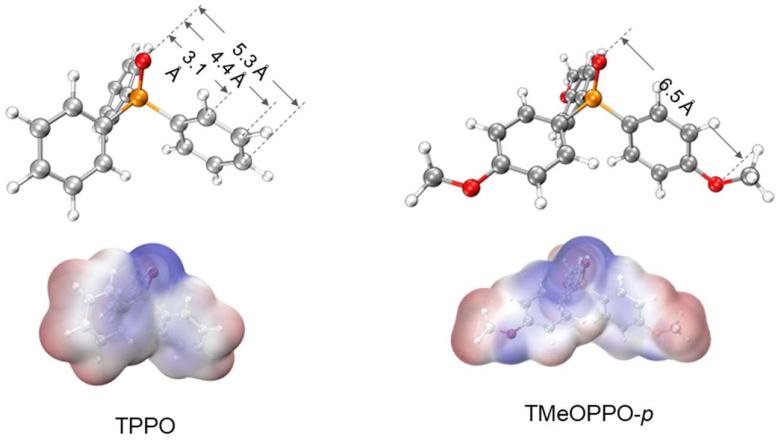


**Fig. R1.2** The calculated ESP of the TPPO and TMeOPPO-*p* molecule.

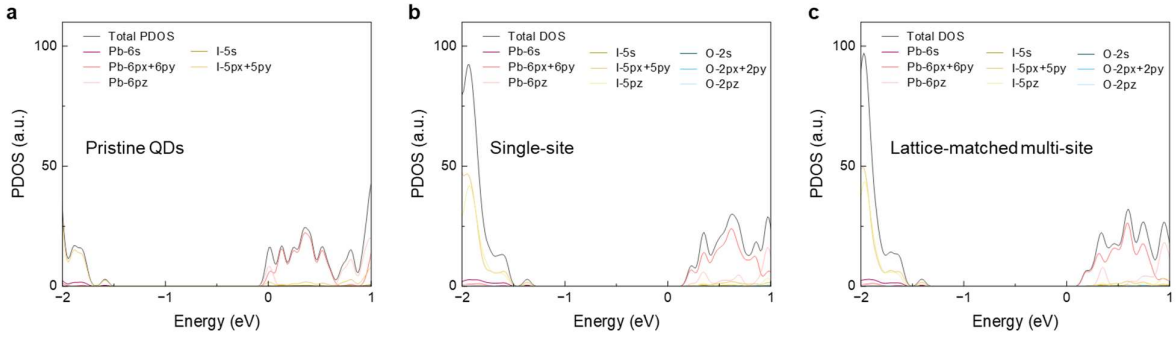


**Fig. R1.3 a**, PDOS of the perovskite QDs with surface defects. **b**, PDOS of the perovskite QDs treated with single-site molecule. **c**, PDOS of the perovskite QDs with multi-site lattice-matched anchoring effect. (**Fig. 1c-d** in the revised manuscript.)

We have now added the corresponding contents and updated the corresponding figures as follows:

**Page 5:** In order to study the effect of site spacing and nucleophilicity on QDs, we synthesised a series of multi-site anchoring molecules, including TMeOPPO-*o*, TMeOPPO-*p*, TFPPO, TClPPO, and TBrPPO (**Fig. 1a**). The site spacing of multi-site anchoring molecules in that order is 2.6 Å, 6.5 Å, 6.6 Å, 7.0 Å and 7.2 Å, respectively. The TMeOPPO-*p* could precisely match the lattice spacing of QDs, allowing it to attach to the surface of the perovskite lattice and provide adequate passivation (**Fig. 1b**). Besides, the nucleophilicity of -$OCH_3$, $F^-$, $Cl^-$ and $Br^-$ decreases in turn, according to the calculated electrostatic potential results. Additionally, the triple-attached nucleophilic groups significantly increase their probability of interacting with uncoordinated $Pb^{2+}$.

**Page 5:** The calculated PDOS revealed that the pristine QDs possess imperfect surface sites featuring a conspicuous trap state originating from halide vacancies or uncoordinated $Pb^{2+}$ $6p_z$ orbital (**Fig. 1c**). We then calculated the PDOSs of single-site anchored (TPPO-treated) QDs. The Pb-$6p_z$ trap states around the Fermi level were eliminated entirely by O-2*p*, whereas the uncoordinated $Pb^{2+}$ maintained the trap states. Meanwhile, the trap peaks were separated from the conduction band minimum (CBM) state, showing that the consecutive trap states could not be eliminated sufficiently (**Fig. 1d**). When the TMeOPPO-*p* offered lattice-matched multi-site anchoring interaction, the trap states and the CBM peaks connected completely, revealing that the P=O and -$OCH_3$ groups from TMeOPPO-*p* could strongly interact with uncoordinated $Pb^{2+}$, stabilise the lattice and eliminate the trap states entirely (**Fig. 1e**). Notably, when the difference between the site spacing of groups and perovskite lattice is too large (i.e., TMeOPPO-*o*), enforced coordination will instead introduce substantial strain, leading to severe structural distortion after optimisation—manifested by anomalous phenomena such as the transformation of benzene rings into five-membered rings. In mismatched multi-site models, failure to enforce passivation at every site results in passivation effects analogous to those in single-site models.

**Page 7:** We first compared the average PLQYs of QD solutions treated with different molecules (concentration of 5 mg $mL^{-1}$ in ethyl acetate). The pristine QD and QDs treated with TPPO, TMeOPPO-*o*, TMeOPPO-*p*, TFPPO, TClPPO, and TBrPPO showed average PLQYs of 59%, 70%, 82%, 96%, 92%, 88%, and 87%, respectively (**Fig. 2a** and **Fig. S2**). The QDs treated with TMeOPPO-*p* showed the highest PLQYs, which is consistent with the theoretical calculation results. TMeOPPO-*p* could offer multi-site anchoring interactions and eliminate defects in QDs (**Fig. 2b**), thus designated as the representative molecule for further exploration and labelled as the "target".

**Page 16:** For example, the devices based on the QDs treated with TPPO, TMeOPPO-*o*, TFPPO, TClPPO and TBrPPO achieved the highest radiance of 49,018 mW Sr $m^{-2}$, 54,821 mW Sr $m^{-2}$, 67,410 mW Sr $m^{-2}$, 85,859 mW Sr $m^{-2}$ and 69,587 mW Sr $m^{-2}$, respectively. The maximum EQEs in that order were 19.79%, 20.16%, 23.62%, 22.38% and 21.45%, respectively. For operating stability, we calculated that the values of $n$ are 1.87, 1.87, 1.87, 1.86, and 1.86 for the devices based on the TPPO-, TMeOPPO-*o*-, TFPPO-, TClPPO- and TBrPPO-treated QDs, respectively. The $T_{50}$ of the devices in that order could be estimated to be 1,944 h, 3,127 h, 8,307 h, 6,139 h and 4,767 h, respectively.

**Page 17**: Combining the results of theoretical calculation, PLQYs and device performance, we can draw the following conclusions: the site spacing and nucleophilicity of groups are the two key factors that would affect the performance of QDs. The closer the site spacing is to the perovskite lattice spacing and the stronger nucleophilicity of the groups, the more stable the lattice and fewer defects in QDs can be achieved, thereby facilitating the fabrication of more efficient and stable QLEDs.

**Comment 2:** In Fig.5, what is the reason for the differences in the QLED performances based on TFPPO, TClPPO, and TBrPPO-treated QDs? The author should discuss the results. I also suggest that authors present three models: single-anchor, multi-anchor, and lattice-matched multi-anchor, to highlight the superiority of the strategy, instead of providing three single-anchor ligands.

**Response:** In the revised manuscript, we have now synthesised ortho-methoxy-substituted TMePPO (TMeOPPO-*o*) and divided all six molecules (TPPO, TMeOPPO-*o*, TMeOPPO-*p*, TFPPO, TClPPO, and TBrPPO) into three types: single-site (TPPO), lattice-mismatched multi-site (TMeOPPO-*o*, TClPPO and TBrPPO) and lattice-matched multi-site (TMeOPPO-*p* and TFPPO).

(i) To study the effect of site spacing and nucleophilicity of groups on QDs and highlight the superiority of the lattice-matched muti-site anchoring effect, we have now tested the anchoring effect of TPPO and TMeOPPO-*o* additionally. We calculated the ESP of TPPO, TMeOPPO-*o*, TMeOPPO-*p*, TFPPO, TClPPO, and TBrPPO (**Fig. R1.4a**). The P=O, halogen and -$OCH_3$ groups all exhibit strong nucleophilicity; thus, these groups can interact strongly with uncoordinated $Pb^{2+}$ through electron-donating effects.

For PDOS calculations (**Fig. R1.4c-e** and **Fig. R1.5**), we applied four models: pristine QDs, QDs with single-site anchors (TPPO), QDs with lattice-mismatched multi-site anchors (TMeOPPO-*o*) and QDs with lattice-matched multi-site anchors (TMeOPPO-*p*). Notably, we also calculated the PDOSs of QDs treated by

lattice-mismatched multi-site molecule (TMeOPPO-*o*). However, when the difference between the site spacing of groups and perovskite lattice is too large (i.e., TMeOPPO-*o*), enforced coordination will instead introduce substantial strain, leading to severe structural distortion after optimisation — manifested by anomalous phenomena such as the transformation of benzene rings into five-membered rings. In mismatched multi-site models, failure to enforce passivation at every site results in passivation effects analogous to those in single-site models. We found that only TMeOPPO-*p* could strongly interact with uncoordinated $Pb^{2+}$, stabilise the lattice and eliminate the trap states entirely.

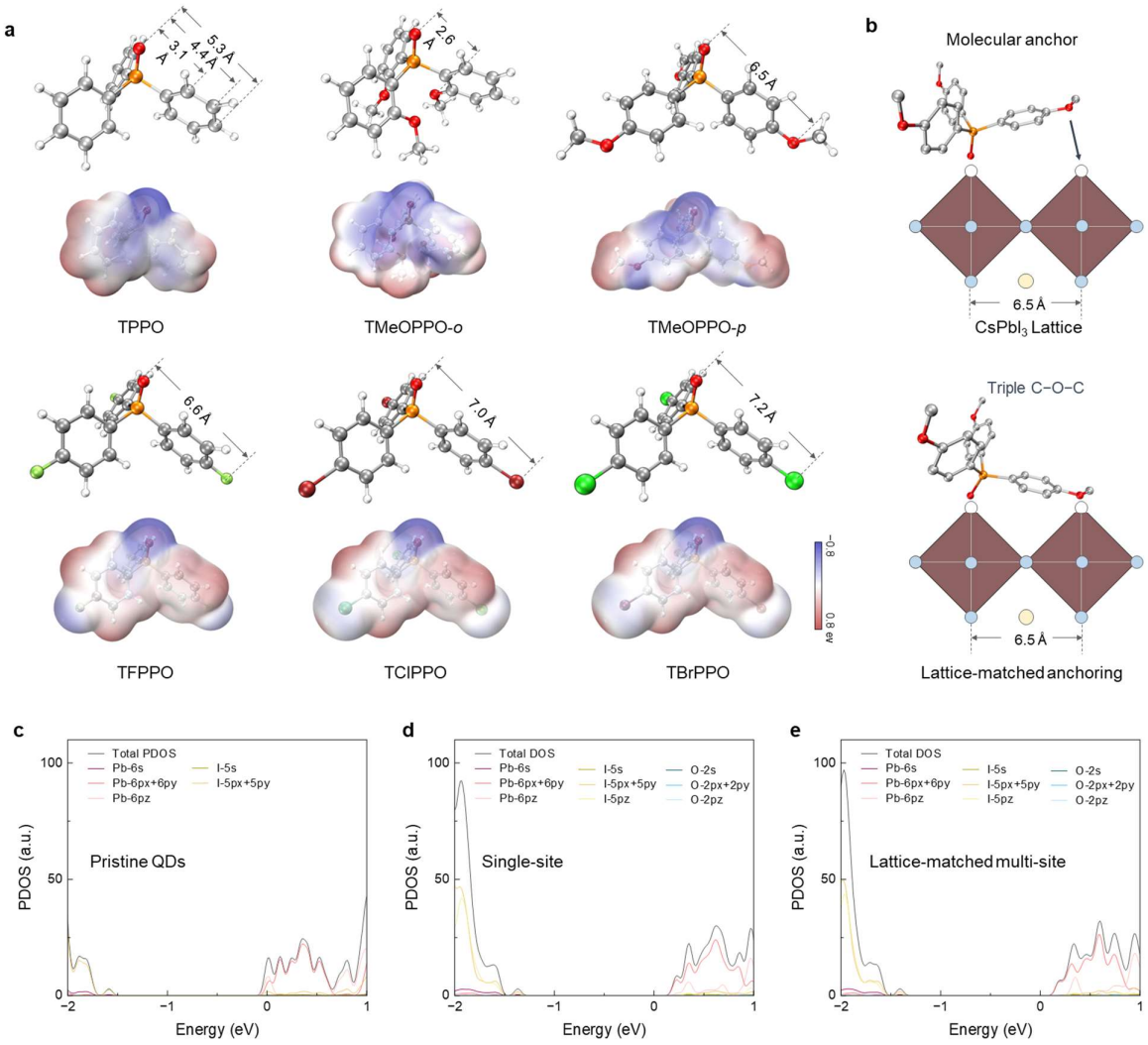


**Fig. R1.4 Lattice-matched multi-site-anchoring strategy. a**, Schematic illustration of lattice-matched anchoring molecule design. **b**, Schematic illustration of the lattice-matched molecular anchoring effect. **c**, PDOS of the perovskite QDs with surface defects. **d**, PDOS of the perovskite QDs treated with single-site molecule. **e**, PDOS of the perovskite QDs with multi-site lattice-matched anchoring effect. (**Fig. 1** in the revised manuscript)

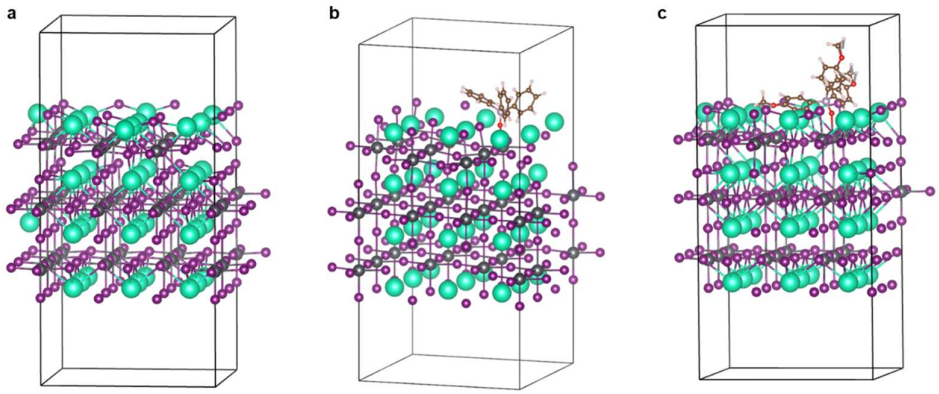


**Fig. R1.5 Crystal models of $CsPbI_3$ for DFT calculation. a**, $CsPbI_3$ with trap defects. **b**, $CsPbI_3$ treated with single-site molecule. **c**, $CsPbI_3$ with lattice-matched multi-site anchoring effect. (**Fig. S1** in the revised Supporting Information)

(ii) We have also compared the average PLQYs of QD solutions treated with different molecules (**Table R1.2**). The pristine QD and QDs treated with TPPO, TMeOPPO-*o*, TMeOPPO-*p*, TFPPO, TClPPO, and TBrPPO showed average PLQYs of 59%, 70%, 82%, 96%, 92%, 88%, and 87%, respectively (**Fig. R1.6**). The as-fabricated QLEDs in that order showed a maximum radiance of 42,809 mW $Sr^{-1}$ $m^{-2}$, 49,018 mW $Sr^{-1}$ $m^{-2}$, 54,821 mW $Sr^{-1}$ $m^{-2}$, 119,037 mW $Sr^{-1}$ $m^{-2}$, 67,410 mW $Sr^{-1}$ $m^{-2}$, 85,859 mW $Sr^{-1}$ $m^{-2}$, 69,587 mW $Sr^{-1}$ $m^{-2}$, a maximum EQE of 15.14%, 19.79%, 20.16%, 26.91%, 23.62%, 22.38%, 22.15%, and a $T_{50}$ of 1,350 h, 1,944 h, 3,127 h, 23,420 h, 8,307 h, 6,139 h, 4,767 h (**Fig. R1.7**), respectively. We have now summarised all data in **Table R1.2**.

According to the results above, we have reached the following conclusions: the site spacing and nucleophilicity of groups are the two key factors that would affect the performance of QDs. The closer the site spacing is to the perovskite lattice spacing and the stronger nucleophilicity of the groups, the more stable the lattice and fewer defects in QDs can be achieved, thereby facilitating the fabrication of more efficient and stable QLEDs. Thus, the superiority of lattice-matched multi-site anchoring molecules has been proved.

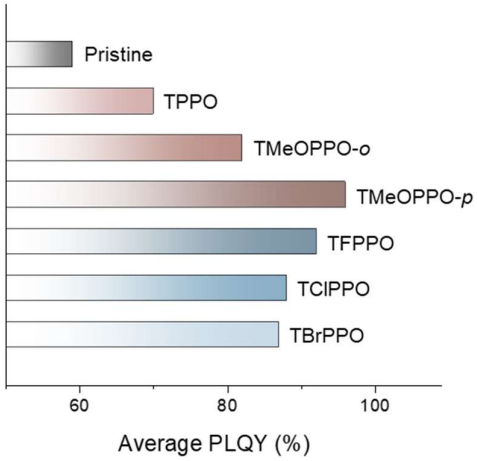


**Fig. R1.6** Average PLQYs of QD solution treated by different molecules. (**Fig. 2a** in the revised manuscript.)

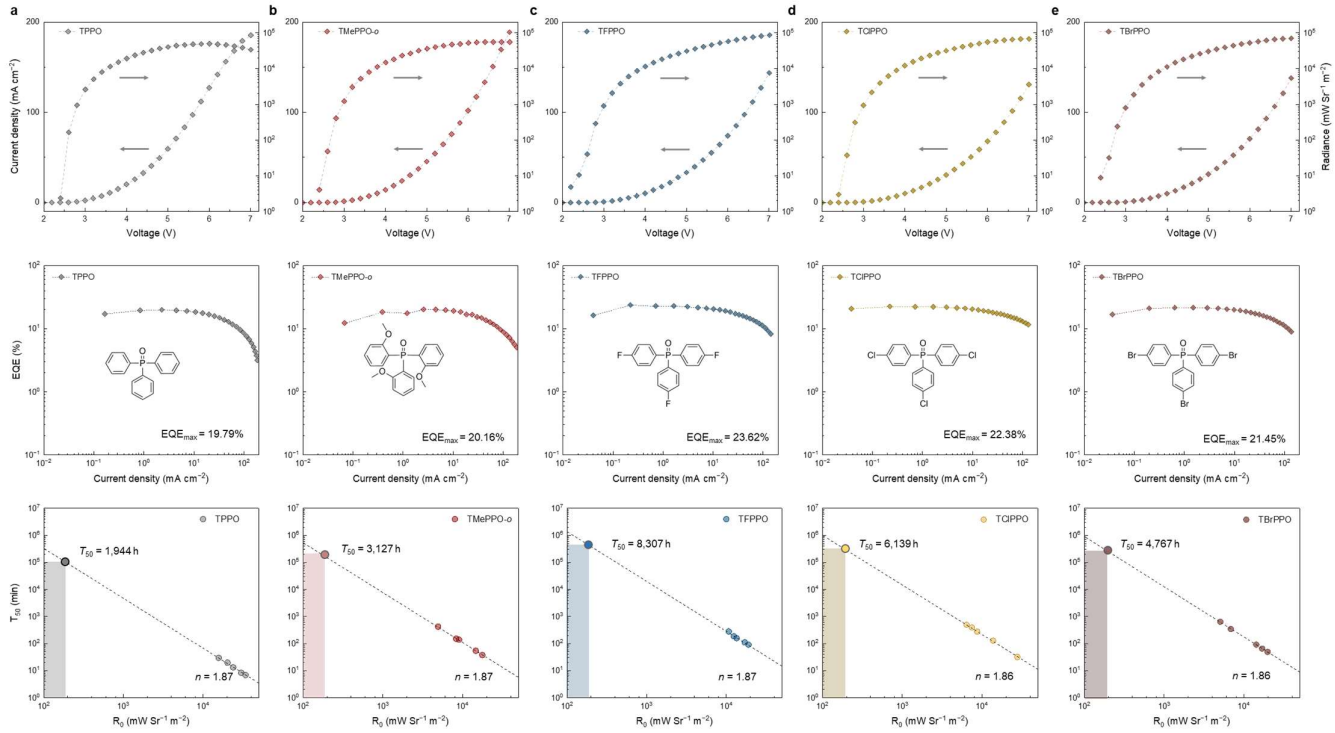


**Fig. R1.7 Performance of QLEDs by using various designed molecules.** Electro-optical conversion performance and stability of QLEDs by using various designed molecules, containing current density-radiance-voltage curve, EQE curve (the insert is the chemical structure) and operating stability. **a**, TPPO. **b**, TMeOPPO-*p*. **c**, TFPPO. **d**, TClPPO. **e**, TBrPPO (**Fig. 6** in the revised manuscript)

**Table R1.2** Device performance of QLEDs with different molecules (**Table 1** in the revised manuscript)

| Device | Type | | Radiance (mW $Sr^{-1}$ $m^{-2}$ ) | $EQE_{max}$ (%) | $EQE_{average}$ (%) | $T_{50}$* (h) |
|---|---|---|---|---|---|---|
| Control | / | / | 42,809 @6.8 V | 15.14 | 12.8 | 1,350 |
| TPPO | Single-site | / | 49,018 @6.0 V | 19.79 | 17.7 | 1,944 |
| TMeOPPO-*o* | Multi-site | Lattice-mismatched | 54,821 @7.0 V | 20.16 | 19.4 | 3,127 |
| TMeOPPO-*p* | Multi-site | Lattice-matched | 119,037 @6.8 V | 26.91 | 25.3 | 23,420 |
| TFPPO | Multi-site | Lattice-matched | 67,410 @7.0 V | 23.62 | 21.8 | 8,307 |
| TClPPO | Multi-site | Lattice-mismatched | 85,859 @7.0 V | 22.38 | 20.3 | 6,139 |
| TBrPPO | Multi-site | Lattice-mismatched | 69,587 @7.0 V | 21.45 | 19.6 | 4,767 |

*For initial radiance of 190 mW $sr^{-1}$ $m^{-2}$, equivalent to a luminance of 100 cd $m^{-2}$ for green perovskite LEDs.

We have now added the corresponding contents and updated the corresponding figures and table as follows:

**Page 5:** In order to study the effect of site spacing and nucleophilicity on QDs, we synthesised a series of multi-site anchoring molecules, including TMeOPPO-*o*, TMeOPPO-*p*, TFPPO, TClPPO, and TBrPPO (**Fig. 1a**). The site spacing of multi-site anchoring molecules in that order is 2.6 Å, 6.5 Å, 6.6 Å, 7.0 Å and 7.2 Å, respectively. The TMeOPPO-*p* could precisely match the lattice spacing of QDs, allowing it to attach to the surface of the perovskite lattice and provide adequate passivation (**Fig. 1b**). Besides, the nucleophilicity of $-OCH_3$, $F^-$, $Cl^-$ and $Br^-$ decreases in turn, according to the calculated electrostatic potential results. Additionally, the triple-attached nucleophilic groups significantly increase their probability of interacting with uncoordinated $Pb^{2+}$.

**Page 5:** The calculated PDOS revealed that the pristine QDs possess imperfect surface sites featuring a conspicuous trap state originating from halide vacancies or uncoordinated $Pb^{2+}$ $6p_z$ orbital (**Fig. 1c**). We then calculated the PDOSs of single-site anchored (TPPO-treated) QDs. The Pb-$6p_z$ trap states around the Fermi level were eliminated entirely by O-2*p*, whereas the uncoordinated $Pb^{2+}$ maintained the trap states. Meanwhile, the trap peaks were separated from the conduction band minimum (CBM) state, showing that the consecutive

trap states could not be eliminated sufficiently (**Fig. 1d**). When the TMeOPPO-*p* offered lattice-matched multi-site anchoring interaction, the trap states and the CBM peaks connected completely, revealing that the P=O and -$OCH_3$ groups from TMeOPPO-*p* could strongly interact with uncoordinated $Pb^{2+}$, stabilise the lattice and eliminate the trap states entirely (**Fig. 1e**). Notably, when the difference between the site spacing of groups and perovskite lattice is too large (i.e., TMeOPPO-*o*), enforced coordination will instead introduce substantial strain, leading to severe structural distortion after optimisation—manifested by anomalous phenomena such as the transformation of benzene rings into five-membered rings. In mismatched multi-site models, failure to enforce passivation at every site results in passivation effects analogous to those in single-site models.

**Page 7:** We first compared the average PLQYs of QD solutions treated with different molecules (concentration of 5 mg $mL^{-1}$ in ethyl acetate). The pristine QD and QDs treated with TPPO, TMeOPPO-*o*, TMeOPPO-*p*, TFPPO, TClPPO, and TBrPPO showed average PLQYs of 59%, 70%, 82%, 96%, 92%, 88%, and 87%, respectively (**Fig. 2a** and **Fig. S2**). The QDs treated with TMeOPPO-*p* showed the highest PLQYs, which is consistent with the theoretical calculation results. TMeOPPO-*p* could offer multi-site anchoring interactions and eliminate defects in QDs (**Fig. 2b**), thus designated as the representative molecule for further exploration and labelled as the "target".

**Page 16:** For example, the devices based on the QDs treated with TPPO, TMeOPPO-*o*, TFPPO, TClPPO and TBrPPO achieved the highest radiance of 49,018 mW Sr $m^{-2}$, 54,821 mW Sr $m^{-2}$, 67,410 mW Sr $m^{-2}$, 85,859 mW Sr $m^{-2}$ and 69,587 mW Sr $m^{-2}$, respectively. The maximum EQEs in that order were 19.79%, 20.16%, 23.62%, 22.38% and 21.45%, respectively. For operating stability, we calculated that the values of *n* are 1.87, 1.87, 1.87, 1.86, and 1.86 for the devices based on the TPPO-, TMeOPPO-*o*-, TFPPO-, TClPPO- and TBrPPO-treated QDs, respectively. The $T_{50}$ of the devices in that order could be estimated to be 1,944 h, 3,127 h, 8,307 h, 6,139 h and 4,767 h, respectively.

**Page 17**: Combining the results of theoretical calculation, PLQYs and device performance, we can draw the following conclusions: the site spacing and nucleophilicity of groups are the two key factors that would affect the performance of QDs. The closer the site spacing is to the perovskite lattice spacing and the stronger nucleophilicity of the groups, the more stable the lattice and fewer defects in QDs can be achieved, thereby facilitating the fabrication of more efficient and stable QLEDs.

**Comment 3:** In DFT results, why were the band gaps of the three models all larger than 2.3 eV, since they

simulate the band structure of $CsPbI_3$ QDs?

**Response:** Thanks to your professional comments, we have now realised the mislead caused by limited computing power in DFT results. Both the VBM and CBM of the unit cell $CsPbI_3$ are located at the R point of the Brillouin zone. They cannot be folded to the Gamma point in a 3×3×3 supercell. However, we performed the 'Gamma point only' k-mesh calculation in the initial manuscript because we found 'no enough memory' error when we adopted a 2×2×2 k-mesh in 3×3×3 supercell optimisation calculations. It cannot obtain the VBM and CBM information in 'Gamma point only' of 3×3×3 supercell calculations due to the performance limitations of the original computer. Hence, the so-called 'bandgaps' as they appear are all larger than 2.3 eV. We have now updated all PDOS results using a 2×2×2 k-mesh calculation on a more powerful supercomputer (**Fig. R1.8** and **Fig. R1.9**).

We have now added the corresponding contents and updated the corresponding figures and table as follows:

**Page 7** in Supporting Information**:** The *k*-mesh and encut were set to 2×2×2 and 50 Ry for structural optimisation, self-consistence field and projected density of state (PDOS) calculations, respectively.

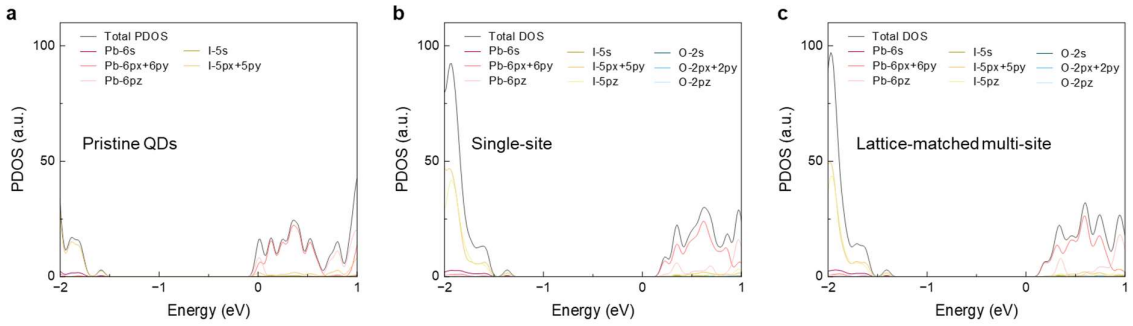


**Fig. R1.8 a**, PDOS of the perovskite QDs with surface defects. **b**, PDOS of the perovskite QDs treated with single-site molecule. **c**, PDOS of the perovskite QDs with multi-site lattice-matched anchoring effect. (**Fig. 1c-d** in the revised manuscript)

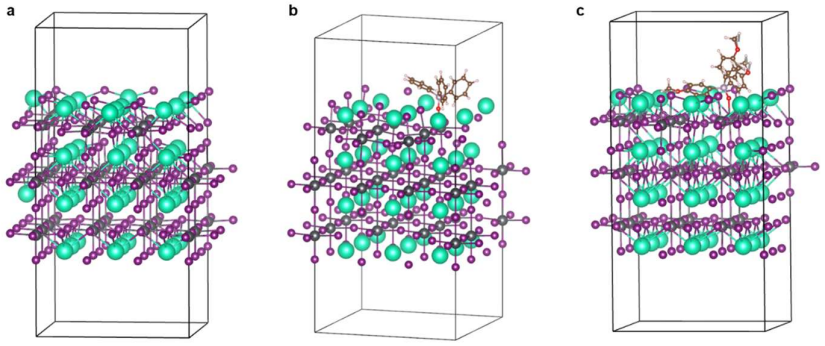

**Fig. R1.9 Crystal models of $CsPbI_3$ for DFT calculation. a**, $CsPbI_3$ with trap defects. **b**, $CsPbI_3$ treated with the single-site molecule. **c**, $CsPbI_3$ with lattice-matched multi-site anchoring effect. (**Fig. S1** in the revised Supporting Information)

**Comment 4:** The air-processed QLEDs based on target QDs could achieve a comparable EQE value with as-fabricated QLEDs. What is the reason for this phenomenon? Can all well-passivated QDs achieve high-performance QLEDs in air? Or is it attributed to the unique properties of TMeOPPO?

**Response:** The instability of perovskite QDs in ambient air arises from two main factors: (i) the dynamic nature of the ligands on the perovskite QDs and (ii) the degradation caused by moisture and oxygen. The interaction between perovskite QDs and ligands exhibits weak binding forces, making it highly dynamic. The loss of ligands would not only lead to aggregation and phase transition of the QDs, but also result in the formation of numerous vacancies on the surface of the QDs. In ambient air, oxygen and moisture would continually attack the defects on the surface of the QD films. Meanwhile, both theoretical calculations and experimental studies have shown that water molecules could easily penetrate the $CsPbI_3$ QD lattice through surface defects, thereby leading to structure degradation. (*Nano Lett. 25, 6192-6199 (2025)*; *Adv. Mater. 35, e2203430 (2023)*)

In this work, we used a series of molecules to eliminate defects and stabilise the lattice of QDs. On the one hand, these molecules could offer strong interaction and replace partial dynamic ligands. On the other hand, these molecules could adhere to the lattice surface and act as a protection layer against moisture and oxygen. Thus, the stability of QLEDs treated by these molecules showed different degrees of improvement. Meanwhile, air-processed QLED still maintained good performance.

To verify the above analysis, we have now added the EL performance of the air-processed QLEDs treated with TFPPO, as shown in **Fig. R1.10**. The air-processed QLED treated with TFPPO exhibited a maximum radiance of 54,841 mW $Sr^{-1}$ $m^{-2}$ and a maximum EQE of 20.14%. It can be concluded that air-processed QLED treated with TFPPO maintained decent EL performance compared with that of QLED processed in nitrogen conditions (EQE of 23.62%). By contrast, the decline of QLED treated with TMePPO-*p* can be considered negligible (from 26.91% to 26.28%). Thus, well-passivated QDs could also achieve high-performance QLEDs in air, whereas TMePPO-*p* showed more prominent resistance to moisture and oxygen due to the stronger nucleophilicity of the -$OCH_3$ group.

We have now added the corresponding contents in the revised manuscript as follows:

**Page 14**: The air-processed QLED exhibited a maximum radiance of 74,356 mW $Sr^{-1}$ $m^{-2}$, a maximum EQE of 26.28% and no EL shift, indicating good oxygen and water resistance and practical application potential for solution processing techniques (**Fig. 5d-f** and **Fig. S11**).

**Page 14**: Besides, the typical air-processed QLED demonstrated good storage stability, which can be attributed to the complete elimination of defects that enhance the resistance of the QD surface to water and oxygen (**Fig. 5g-i**).

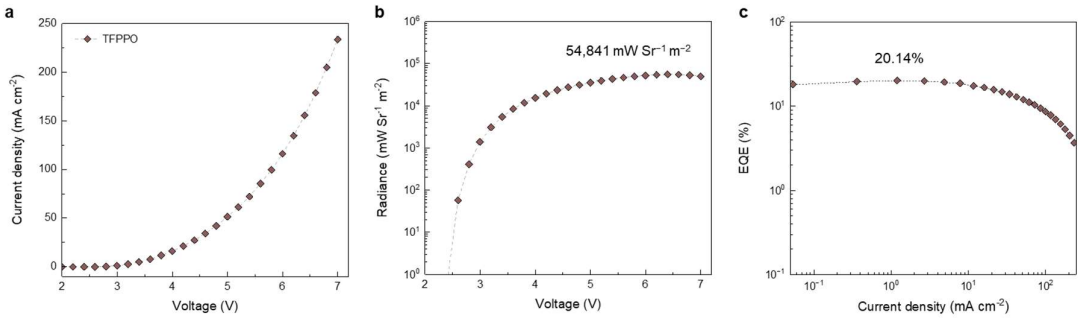


**Fig. R1.10** The EL performance of air-processed QLED treated with TFPPO. **a**, Current density-voltage curve. **b**, Voltage-radiance curve. **c**, EQE curve. (**Fig. S11** in the revised Supporting Information)

**Comment 5:** Why is the surface ligand density of target QDs lower (line 157) than control QDs? Since TMeOPPO shows stronger coordination with surface $Pb^{2+}$, it seems they are more tightly bound to the surface and harder to be washed than OA/OAm during purification.

**Response:** QDs have quite a large surface-to-volume ratio due to their small particle size, resulting in considerable surface energy and high activity. Thus, QDs require ligands to bind to their surface in order to retain colloidal stability. Surface ligands play a dual role in restricting and protecting QDs. (*Adv. Mater. 30, 1800764 (2018); Adv. Mater. 29, 1603885 (2017)*). To simultaneously achieve high PLQYs, good film-forming properties and good electrical conductivity for QDs, OA/OAm ligands with rational amounts are necessary.

In this work, we used polar solvents to wash away the excess ligands, thereby achieving QDs with a rational ligand density. The interaction between ligands (OA/OAm) and the QD surface is highly dynamic and labile, allowing ligands to easily fall off during the QDs' purification and storage processes. We added TMeOPPO during the QDs' second-round purification process, and TMeOPPO-*p* would preferentially bind to the QD

surface because of its stronger coordination, making partial dynamic OA/OAm ligands more easily washed (**Fig. R1.11**). In the FITR and NMR results, we find that TMeOPPO-*p* could adhere to the QD surface, and the density of OA/OAm in target QDs is lower than that of pristine QDs (**Fig. R1.12**).

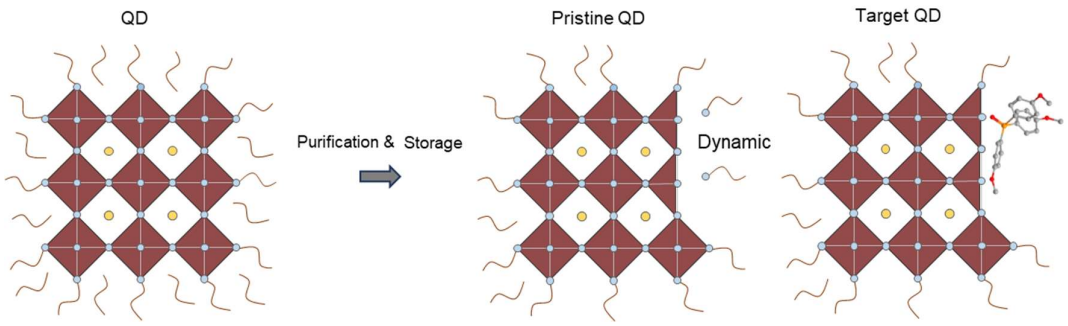


**Fig. R1.11** Schematic illustration of purification and storage processes of QDs.

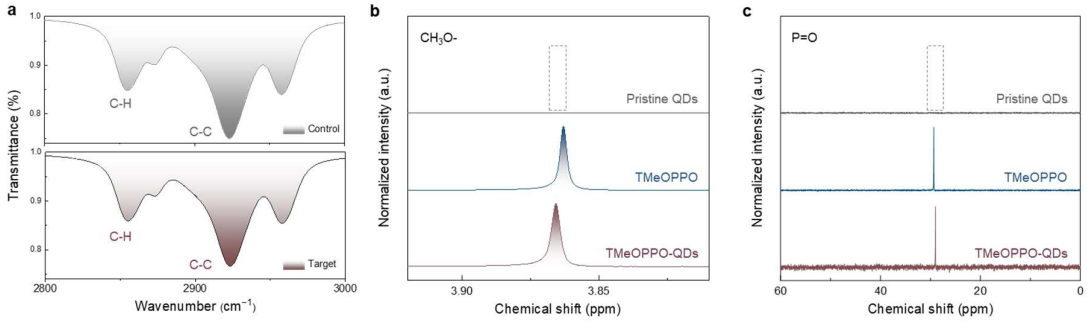


**Fig. R1.12 a**, FTIR spectra of the QDs. **b**, $^{1}$H NMR spectra of the pristine QDs, TMeOPPO-*p*, and target QDs. **c**, $^{31}$P NMR spectra of the pristine QDs, TMeOPPO-*p*, and target QDs.

**Comment 6:** Why are the hole trap densities of both control and target QDs so high, about $10^{18}$ cm$^{-3}$, even three-order higher than other reported $CsPbI_3$ QDs?

**Response:** We fabricated hole-only devices based on the control and target QDs and calculated the hole trap density of the devices by using the equation $N = 2\varepsilon_0\varepsilon_r V_{TFL}/eL^2$. The $\varepsilon_0$ is Vacuum Permittivity, and its value is $8.85 \times 10^{-12}$ F m$^{-1}$. The $\varepsilon_r$ is the relative permittivity of perovskite (6.32 for $CsPbI_3$, *Nano Lett. 20, 2829 (2020)*). The $e$ is the elementary charge ($1.6 \times 10^{-19}$ C). The thickness of the QD layer is 20~40 nm. Thus, the $N_{trap}$ is determined by $V_{TFL}$ (0.1~1 V).

The reasonable order range of $N_{trap}$ should be within $10^{23}$~$10^{24}$ m$^{-3}$ (or $10^{17}$~$10^{18}$ cm$^{-3}$). We made a summary of the reported $V_{TFL}$ and $N_{trap}$ data for $CsPbI_3$ QDs over the past two years (**Table R1.3**), and found that our results are reasonable and consistent with other reports ($10^{17}$~$10^{18}$ cm$^{-3}$).

**Table R1.3** The characteristics of reported $CsPbI_3$ QDs.

| Type | $V_{TFL}$ (V) | $N_{trap}$ ($cm^{-3}$) | Ref. |
|---|---|---|---|
| Pristine $CsPbI_3$ QD | 0.43 | $7.53 \times 10^{17}$ | *Angew. Chem. Int. Ed.* **63**, e202318777 (2024) |
| Target $CsPbI_3$ QD | 0.16 | $2.79 \times 10^{17}$ | |
| Pristine $CsPbI_3$ QD | 0.39 | $5.80 \times 10^{17}$ | *Nano Lett.* **25**, 6192-6199 (2025) |
| Target $CsPbI_3$ QD | 0.15 | $2.23 \times 10^{17}$ | |
| Pristine $CsPbI_3$ QD | / | $4.66 \times 10^{18}$ | *Adv. Funct. Mater.* 2311554 (2024). |
| FA doped $CsPbI_3$ QD | / | $1.75 \times 10^{18}$ | |
| Target $CsPbI_3$ QD | / | $1.15 \times 10^{18}$ | |
| Pristine $CsPbI_3$ QD | 0.74 | ~$1.10 \times 10^{18}$ | *Sci. Adv.*, eado7159 (2025) |
| Target $CsPbI_3$ QD | 0.64 | ~$9.55 \times 10^{17}$ | |
| Pristine $CsPbI_3$ QD | 0.71 | $1.06 \times 10^{18}$ | This work |
| Target $CsPbI_3$ QD | 0.45 | $6.69 \times 10^{17}$ | |

**Comment 7:** The *J-V* curve of the control QLED looks abnormal. The authors also mentioned that the target QLEDs yield a 3-fold radiance of the control device at 6.8 V (Line 183), but the current density of target QLEDs at 6.8 V is 5 times larger than that of control QLEDs (Fig. 4d). This result seems inconsistent with the EQE curves.

**Response:**

(i) Due to the high ligand density and numerous defects in pristine QDs, the charge transfer in the control QLED is not smooth. Thus, for the control QLED, the rate of increase in current density is relatively slow, which is a common phenomenon observed in experiments.

(ii) The control device showed a current density of 76.5 mA $cm^{-2}$, a radiance of 42,809 mW Sr $m^{-2}$ and an EQE of 9.76% at 6.8 V. For comparison, the target device showed a current density of 216.1 mA $cm^{-2}$, a radiance of 119,037 mW Sr $m^{-2}$ and an EQE of 9.64% at 6.8 V. The radiance of the target device is 2.78 times that of the control device, while the current density of the target device is 2.82 times that of the control device, which enables similar EQE values at 6.8 V. Thus, the result is consistent with the EQE curves (**Table R1.4**).

**Table R1.4** The characteristics of the control and target devices under 6.8 V.

| | Radiance | Current density | EQE |
|---|---|---|---|
| Control device | 42,809 mW Sr $m^{-2}$ | 76.5 mA $cm^{-2}$ | 9.76% |
| Target device | 119,037 mW Sr $m^{-2}$ | 216.1 mA $cm^{-2}$ | 9.64% |

**Comment 8:** Fig.5c has not summarised a recent reported high-performance QLEDs (Sci. Adv. 2025, 11, eads7159).

**Response:** We have now updated **Fig. 5c** (**Fig. R1.13**) as follows.

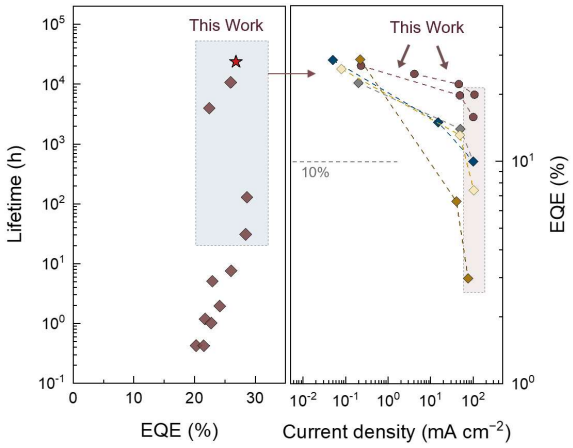


**Fig. R1.13** Summary of the reported red perovskite LED characteristics based on maximum EQE, $T_{50}$ and roll-off. (**Fig. 5c** in the revised manuscript.)

## Replies to Reviewer #2

**Comments to the Author:**

In this work, Chen et al. designed a new molecule according to the lattice characteristics of perovskite quantum dots. The lattice-matched molecular anchor enables QLED with a high EQE of 27% and excellent stability under operation, high current density and water-oxygen environment. Overall, this work could useful to the broad community working on optoelectronic properties of perovskites and inspire researchers to design molecules on demand. I am supportive of publication in Nature Communications after addressing following concerns.

**Comment 1:** The authors chose TPPO as the basic molecular framework, and I noticed that TPPO should also have an enhancing effect on the performance of the device theoretically. Please conduct the TPPO-treated QLEDs.

**Response:** Thank you for your suggeations. We have conducted TPPO-treated QLEDs and demonstrated the device performance and operating stability (**Fig. R2.1**). The TPPO-treated QLED showed a maximum radiance of 49,018 mW $Sr^{-1}$ $m^{-2}$, a maximum EQE of 19.79% and a $T_{50}$ of 1,944 h. It can be concluded that QLED based on TPPO-treated QDs showed better EL performance and operating stability compared to the control device, but not as good as QLED based on TMeOPPO-*p*-treated QDs. The results confirmed the superiority of our proposed lattice-matched multi-site anchoring effect.

We have now updated **Fig. 6** (**Fig. R2.2**), **Table 1** (**Table R2.1**) and added the corresponding contents in the revised manuscript as follows:

**Page 16**: For example, the devices based on the QDs treated with TPPO, TMeOPPO-*o*, TFPPO, TClPPO and TBrPPO achieved the highest radiance of 49,018 mW Sr $m^{-2}$, 54,821 mW Sr $m^{-2}$, 67,410 mW Sr $m^{-2}$, 85,859 mW Sr $m^{-2}$ and 69,587 mW Sr $m^{-2}$, respectively. The maximum EQEs in that order were 19.79%, 20.16%, 23.62%, 22.38% and 21.45%. For operating stability, we calculated that the values of *n* are 1.87, 1.87, 1.87, 1.86, and 1.86 for the devices based on the TPPO-, TMeOPPO-*o*-, TFPPO-, TClPPO- and TBrPPO-treated QDs, respectively. The $T_{50}$ for the devices in that order could be estimated to be 1,944 h, 3,127 h, 8,307 h, 6,139 h and 4,767 h, respectively.

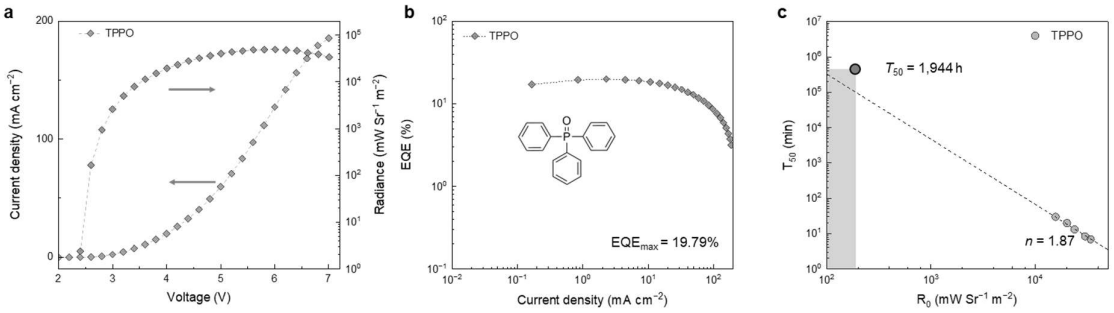


**Fig. R2.1** Electro-optical conversion performance and stability of QLEDs by using TPPO, containing current density-radiance-voltage curve, EQE curve (the insert is the chemical structure) and operating stability.

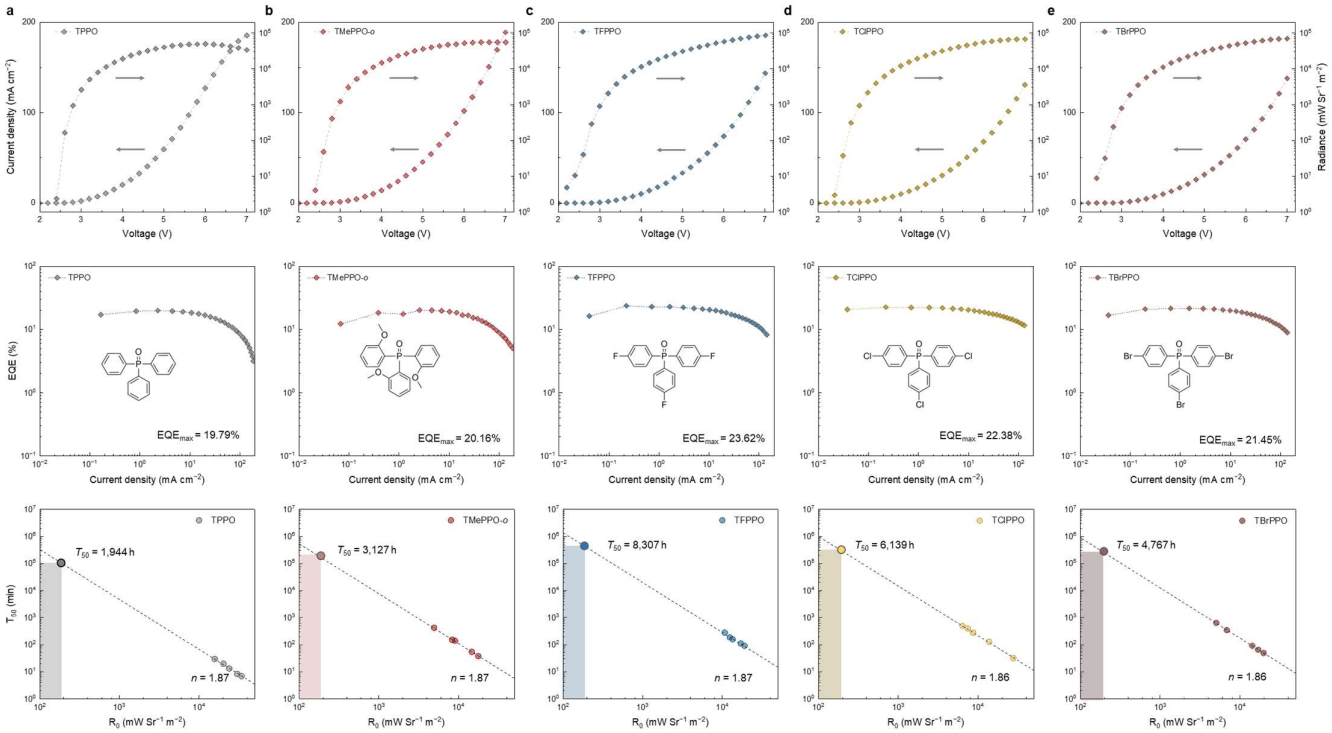


**Fig. R2.2 Performance of QLEDs by using various designed molecules.** Electro-optical conversion performance and stability of QLEDs by using various designed molecules, containing current density-radiance-voltage curve, EQE curve (the insert is the chemical structure) and operating stability. **a**, TPPO. **b**, TMeOPPO-*p*. **c**, TFPPO. **d**, TClPPO. **e**, TBrPPO. (**Fig. 6** in the revised manuscript)

**Table R2.1** Device performance of QLEDs with different molecules (Table 1 in the revised manuscript)

| Device | Type | | Radiance (mW $Sr^{-1}$ $m^{-2}$ ) | $EQE_{max}$ (%) | $EQE_{average}$ (%) | $T_{50}$* (h) |
|---|---|---|---|---|---|---|
| Control | / | / | 42,809 @6.8 V | 15.14 | 12.8 | 1,350 |
| TPPO | Single-site | / | 49,018 @6.0 V | 19.79 | 17.7 | 1,944 |
| TMeOPPO-*o* | Multi-site | Lattice-mismatched | 54,821 @7.0 V | 20.16 | 19.4 | 3,127 |
| TMeOPPO-*p* | Multi-site | Lattice-matched | 119,037 @6.8 V | 26.91 | 25.3 | 23,420 |
| TFPPO | Multi-site | Lattice-matched | 67,410 @7.0 V | 23.62 | 21.8 | 8,307 |
| TClPPO | Multi-site | Lattice-mismatched | 85,859 @7.0 V | 22.38 | 20.3 | 6,139 |
| TBrPPO | Multi-site | Lattice-mismatched | 69,587 @7.0 V | 21.45 | 19.6 | 4,767 |

*For initial radiance of 190 mW $sr^{-1}$ $m^{-2}$, equivalent to a luminance of 100 cd $m^{-2}$ for green perovskite LEDs.

**Comment 2:** I am very interested in the EQE changes of the air-processed QLED after being stored for some time. Please provide relevant experiments to verify the storage stability of air-processed QLED, as well as detailed preparation conditions for the air-processed QLED, especially the air humidity.

**Response:** As suggested, we have tested the air-processed QLED after being stored for one and two weeks, as shown in **Fig. R2.2**. The typical air-processed QLED demonstrated an EQE of 25.65%, and it maintained an EQE of 24.82% after being stored for one week (23.73% for two weeks). These results indicated that the air-processed QLED has excellent storage stability, which can be attributed to the elimination of defects that enhance the resistance of the QD surface to water and oxygen.

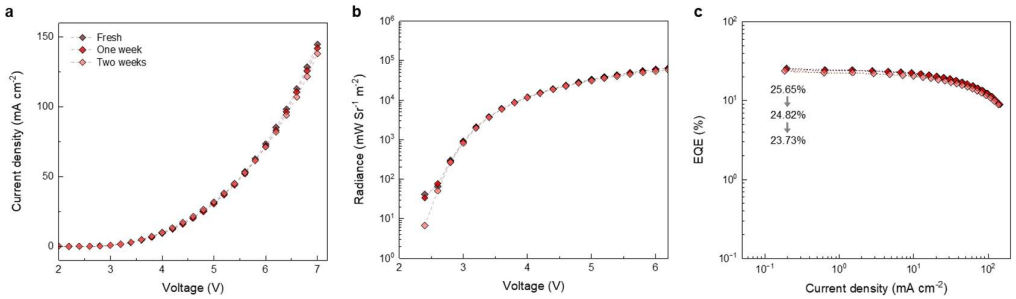

**Fig. R2.2** The storage stability of typical air-processed QLED. **g**, Current density-voltage curves of QLED after 0/1/2 weeks storage. **h**, Voltage-radiance curves of QLED after 0/1/2 week storage. **i**, EQE curves of QLED after 0/1/2 weeks storage.

We have now added the corresponding contents and updated the corresponding figure in the revised manuscript as follows:

**Page 14**: Besides, the typical air-processed QLED demonstrated good storage stability, which can be attributed to the complete elimination of defects that enhance the resistance of the QD surface to water and oxygen (**Fig. 5g-i**).

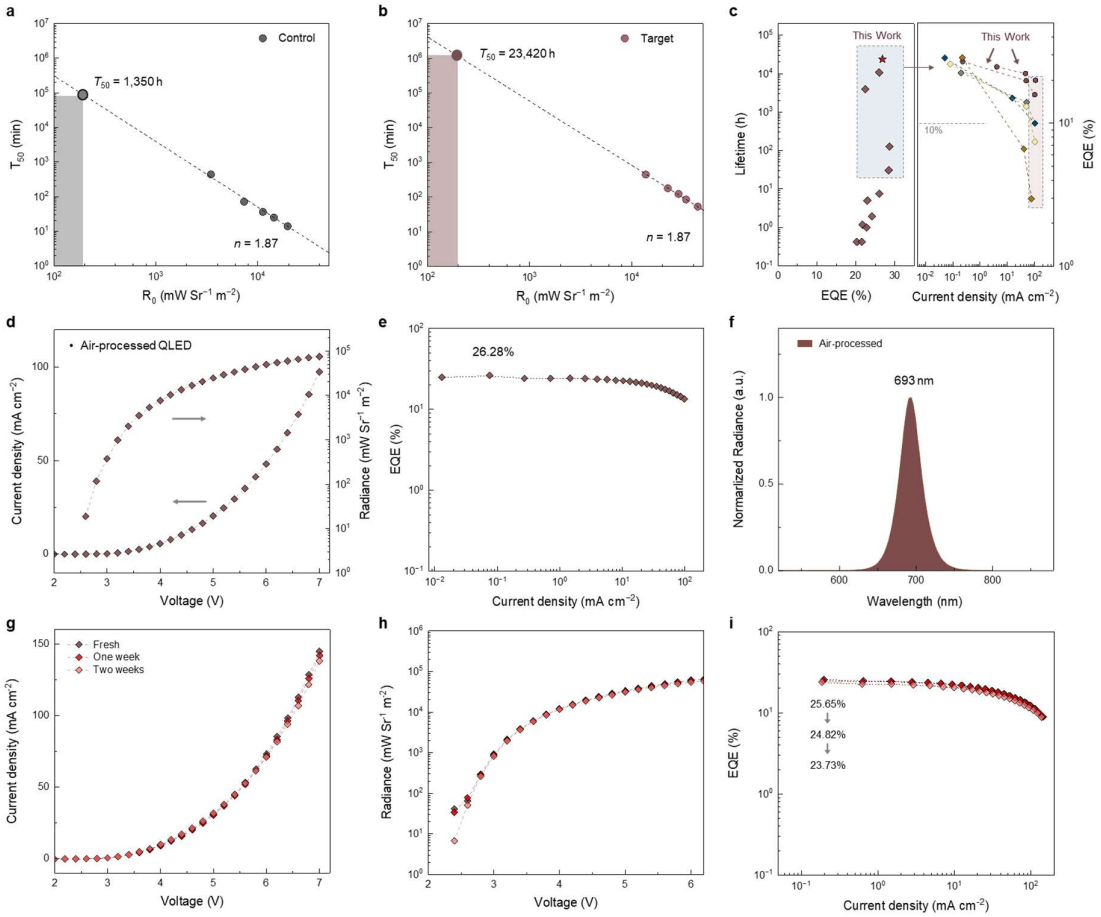


**Fig. R2.3 Stability of QLEDs.** The $T_{50}$ lifetimes as a function of $R_0$ for the control and target QLEDs. The dashed line fits the $T_{50}$ data to the equation $R_0^n$ $T_{50}$ = Constant, where n is the acceleration factor. **a**, the control device. **b**, the target device. **c**, Summary of the reported red perovskite LED characteristics based on maximum EQE, $T_{50}$ and roll-off. **d-f,** EL performance of air-processed champion QLED. **d**, Current density-voltage-radiance curve. **e**, EQE curve. **f**, EL

spectra. **g-i**, The storage stability of a typical air-processed QLED. **g**, Current density-voltage curves of QLED after 0/1/2 weeks of storage. **h**, Voltage-radiance curves of QLED after 0/1/2 weeks of storage. **i**, EQE curves of QLED after 0/1/2 weeks of storage. (**Fig. 5** in the revised manuscript)

**Comment 3:** In Figures 2f and g, the $^{1}$H NMR spectra of the target QDs showed a higher chemical shift, while the $^{31}$P NMR spectra of the target QDs showed a lower chemical shift. Please provide a detailed explanation.

**Response:** The P=O bond in TMeOPPO-*p* coordinated with $Pb^{2+}$ in the form of a double bond. This process not only formed a sigma coordination bond but also allowed the d orbitals of the Pb atom to interact with the π*-antibonding orbital of the double bond, creating a π backbonding. This delocalised the charge on the Pb and increased the π-electron density, thereby slightly shifting the $^{31}$P NMR peak upfield. In contrast, when the methoxy group bound to Pb, no π backbonding was formed, resulting in a reduction of the electron cloud density around the hydrogen atoms and a downfield shift in the $^{1}$H NMR peak. These results further confirmed our lattice-matched anchoring effect on QDs.

We have now added the corresponding contents in the revised manuscript as follows:

**Page 8**: Notably, the $^{1}$H NMR spectra of the target QDs showed a higher chemical shift, while the $^{31}$P NMR spectra of the target QDs showed a lower chemical shift. The P=O bond in TMeOPPO-*p* coordinated with $Pb^{2+}$ in the form of a double bond. This process not only formed a sigma coordination bond but also allowed the d orbitals of the Pb atom to interact with the π*-antibonding orbital of the double bond, creating a π backbonding. This delocalised the charge on the Pb and increased the π-electron density, thereby slightly shifting the $^{31}$P NMR peak upfield. In contrast, when the methoxy group bound to Pb, no π backbonding was formed, resulting in a reduction of the electron cloud density around the hydrogen atoms and a downfield shift in the $^{1}$H NMR peak.

**Comment 4:** Please provide the fitting details (bi-exponential or tri-exponential equation) for TRPL measurements.

**Response:** We fitted the decay curves by applying the bi-exponential equation: $I = A_1\, exp\left(-\frac{t}{\tau_1}\right) + A_2\, exp\left(-\frac{t}{\tau_2}\right)$. We calculated the average PL lifetime by using the equation: $\tau_{avg} = \frac{A_1{\tau_1}^2 + A_2{\tau_2}^2}{A_1\tau_1 + A_2\tau_2}$.

We have now added the corresponding contents in the revised Supporting Information as follows:

**Page 8** in Supporting Information: The decay curves were fitted by applying the bi-exponential equation: $I = A_1\, exp\left(-\frac{t}{\tau_1}\right) + A_2\, exp\left(-\frac{t}{\tau_2}\right)$. The average PL lifetime was calculated by: $\tau_{avg} = \frac{A_1{\tau_1}^2 + A_2{\tau_2}^2}{A_1\tau_1 + A_2\tau_2}$.

**Comment 5:** Could the molecular anchor stabilise octahedrons and maintain lattice stability, thereby inhibiting ionic migration?

**Response:** The ion migration and the twisting of the octahedron under the electric field are the root causes of the high efficiency roll-off of perovskite LEDs (*Nat. Commun. 12, 5081 (2021)*). In this work, we applied TMeOPPO-*p* to offer lattice-matched multi-site anchoring interactions, thereby stabilising the lattice and inhibiting ion migration. The theoretical calculation results indicated that the P=O and -$OCH_3$ groups from TMeOPPO-*p* could strongly interact with uncoordinated $Pb^{2+}$, stabilising the lattice and eliminating the trap states entirely (**Fig. R2.4**). Besides, the target QLED demonstrated a very small efficiency roll-off (i.e., over 20% EQE at a current density of 100 mA $cm^{-2}$) and a nearly 20-fold increase in operating stability. Thus, we agree with the reviewer that the TMeOPPO-*p* could stabilise octahedrons and maintain lattice stability, thereby inhibiting ionic migration and achieving small efficiency roll-off.

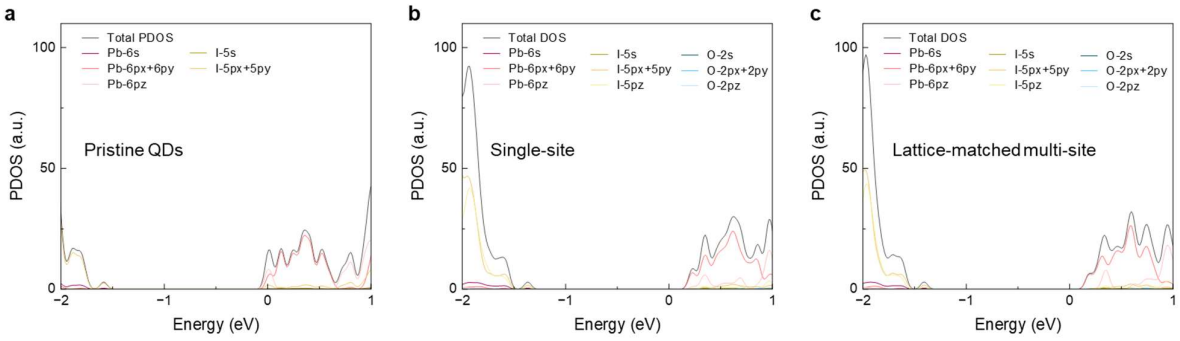


**Fig. R2.4 a**, PDOS of the perovskite QDs with surface defects. **b**, PDOS of the perovskite QDs treated with single-site molecule. **c**, PDOS of the perovskite QDs with multi-site lattice-matched anchoring effect. (**Fig. 1c-d** in the revised manuscript)

We have now added the corresponding discussions in the revised manuscript as follows:

**Page 5**: When the TMeOPPO-*p* offered lattice-matched multi-site anchoring interaction, the trap states and the CBM peaks connected completely, revealing that the P=O and -$OCH_3$ groups from TMeOPPO-*p* could strongly interact with uncoordinated $Pb^{2+}$, stabilise the lattice and eliminate the trap states entirely (**Fig. 1e**). Notably, if the difference between the site spacing of groups and perovskite lattice is too large (i.e.,

TMeOPPO-*o*), enforced coordination will instead introduce substantial strain, leading to severe structural distortion after optimisation—manifested by anomalous phenomena such as the transformation of benzene rings into five-membered rings. In mismatched multi-site models, failure to enforce passivation at every site results in passivation effects analogous to those in single-site models.

**Page 14**: Benefiting from the stabilised lattice and inhibited ion migration in QDs, the target QLEDs show ultra-low efficiency roll-off at high current densities.

**Comment 6:** The descriptions of the type of ligands should be checked carefully. For example, does the halogen in TFPPO participate in passivation? If so, the ligand type description in the manuscript and Table 1 should be carefully reviewed. If not, a clear rationale for comparing the lengths of different groups in the F-substituted ligand is required. Other ligands are the same as TFPPO.

**Response:** In the revised manuscript, we have synthesised TMeOPPO-*o* additionally and divided all six molecules (TPPO, TMeOPPO-*o*, TMeOPPO-*p*, TFPPO, TClPPO, and TBrPPO) into three types: single-site (TPPO), lattice-mismatched multi-site (TMeOPPO-*o*, TClPPO and TBrPPO) and lattice-matched multi-site (TMeOPPO-*p* and TFPPO).

We calculated the ESP of TFPPO, TClPPO, and TBrPPO. The halogen groups also have strong nucleophilicity, as shown in **Fig. R2.5**. The nucleophilicity of -F, -Cl and -Br decreases successively. The site spacing of TFPPO (6.6 Å) is very close to the lattice spacing of the perovskite (6.5 Å), regarded as lattice-matched multi-site anchoring molecules, while TClPPO and TBrPPO are regarded as lattice-mismatched multi-site anchoring molecules. We updated the descriptions of the type of ligands in the manuscript and **Table 1** (**Table R2.2**).

We have also compared the average PLQYs of QD solutions treated with different molecules. The pristine QD and QDs treated with TPPO, TMeOPPO-*o*, TMeOPPO-*p*, TFPPO, TClPPO, and TBrPPO showed average PLQYs of 59%, 70%, 82%, 96%, 92%, 88%, and 87%, respectively (**Fig. R2.6** and **Fig. R2.7**). The as-fabricated QLEDs in that order showed a maximum radiance of 42,809 mW $Sr^{-1}$ $m^{-2}$, 49,018 mW $Sr^{-1}$ $m^{-2}$, 54,821 mW $Sr^{-1}$ $m^{-2}$, 119,037 mW $Sr^{-1}$ $m^{-2}$, 67,410 mW $Sr^{-1}$ $m^{-2}$, 85,859 mW $Sr^{-1}$ $m^{-2}$, 69,587 mW $Sr^{-1}$ $m^{-2}$, a maximum EQE of 15.14%, 19.79%, 20.16%, 26.91%, 23.62%, 22.38%, 22.15%, and a $T_{50}$ of 1,350 h, 1,944 h, 3,127 h, 23,420 h, 8,307 h, 6,139 h, 4,767 h (**Fig. R2.8**), respectively. We have now summarised all data in **Table R1.2**.

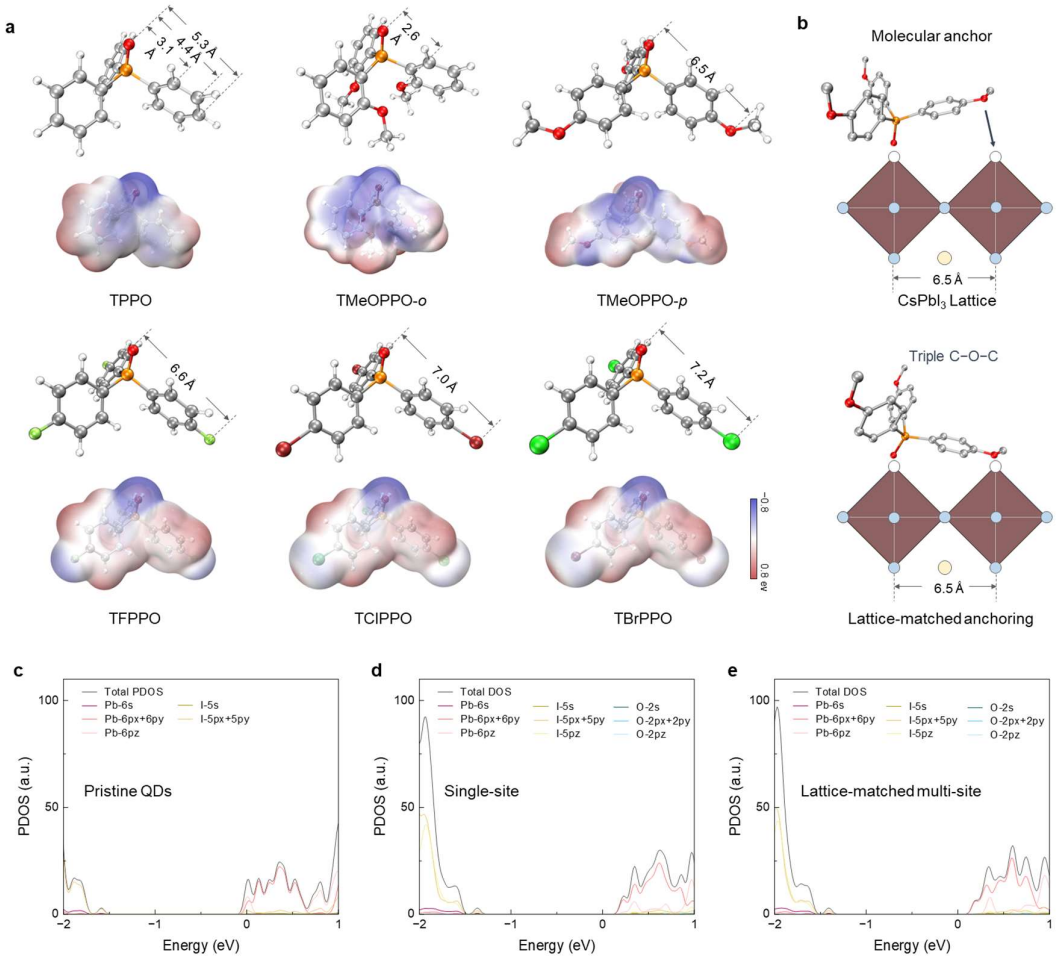


**Fig. R2.5 Lattice-matched multi-site-anchoring strategy. a**, Schematic illustration of lattice-matched anchoring molecule design. **b**, Schematic illustration of the lattice-matched molecular anchoring effect. **c**, PDOS of the perovskite QDs with surface defects. **d**, PDOS of the perovskite QDs treated with single-site molecule. **e**, PDOS of the perovskite QDs with multi-site lattice-matched anchoring effect. (**Fig. 1** in the revised manuscript)

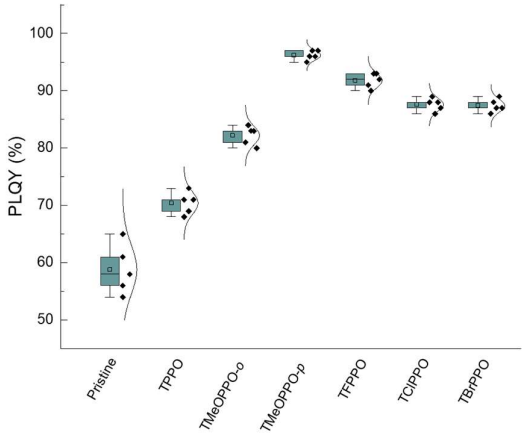


**Fig. R2.6** PLQYs of QD solution treated by different molecules. (**Fig. S2** in the revised Supporting Information)

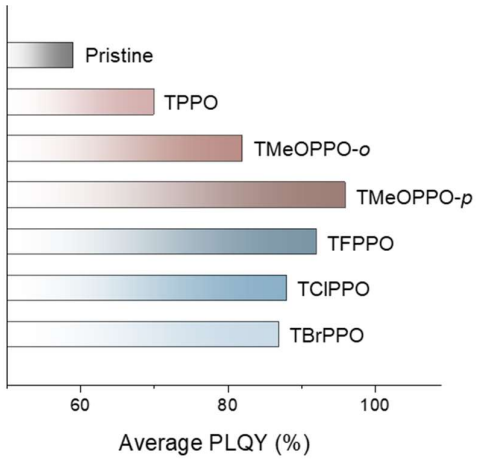


**Fig. R2.7** Average PLQYs of QD solution treated by different molecules. (**Fig. 2a** in the revised manuscript.)

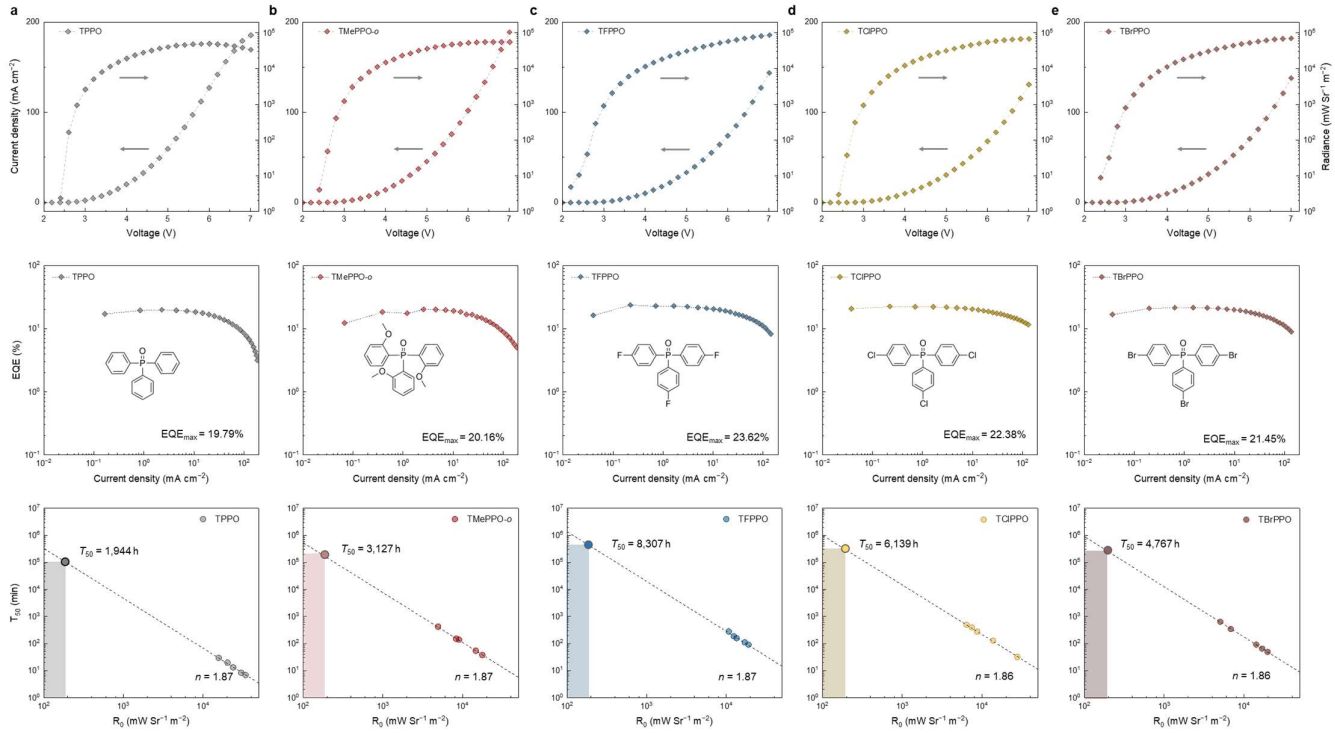


**Fig. R2.8 Performance of QLEDs by using various designed molecules.** Electro-optical conversion performance and stability of QLEDs by using various designed molecules, containing current density-radiance-voltage curve, EQE curve (the insert is the chemical structure) and operating stability. **a**, TPPO. **b**, TMeOPPO-*p*. **c**, TFPPO. **d**, TClPPO. **e**, TBrPPO (**Fig. 6** in the revised manuscript)

**Table R2.2** Device performance of QLEDs with different molecules (**Table 1** in the revised manuscript)

| Device | Type | | Radiance (mW $Sr^{-1}$ $m^{-2}$ ) | $EQE_{max}$ (%) | $EQE_{average}$ (%) | $T_{50}$* (h) |
|---|---|---|---|---|---|---|
| Control | / | / | 42,809 @6.8 V | 15.14 | 12.8 | 1,350 |
| TPPO | Single-site | / | 49,018 @6.0 V | 19.79 | 17.7 | 1,944 |
| TMeOPPO-*o* | Multi-site | Lattice-mismatched | 54,821 @7.0 V | 20.16 | 19.4 | 3,127 |
| TMeOPPO-*p* | Multi-site | Lattice-matched | 119,037 @6.8 V | 26.91 | 25.3 | 23,420 |
| TFPPO | Multi-site | Lattice-matched | 67,410 @7.0 V | 23.62 | 21.8 | 8,307 |
| TClPPO | Multi-site | Lattice-mismatched | 85,859 @7.0 V | 22.38 | 20.3 | 6,139 |
| TBrPPO | Multi-site | Lattice-mismatched | 69,587 @7.0 V | 21.45 | 19.6 | 4,767 |

*For initial radiance of 190 mW $sr^{-1}$ $m^{-2}$, equivalent to a luminance of 100 cd $m^{-2}$ for green perovskite LEDs.

We have concluded that the site spacing and nucleophilicity of groups are the two key factors that affect the performance of QDs and QLEDs. The closer the site spacing is to the perovskite lattice spacing and the stronger nucleophilicity of the groups, the more stable the lattice and fewer defects in QDs can be achieved, thereby facilitating the fabrication of more efficient and stable QLEDs.

We have now added the corresponding contents and updated the corresponding figures and table as follows:

**Page 5:** In order to study the effect of site spacing and nucleophilicity on QDs, we synthesised a series of multi-site anchoring molecules, including TMeOPPO-*o*, TMeOPPO-*p*, TFPPO, TClPPO, and TBrPPO (**Fig. 1a**). The site spacing of multi-site anchoring molecules in that order is 2.6 Å, 6.5 Å, 6.6 Å, 7.0 Å and 7.2 Å, respectively. The TMeOPPO-*p* could precisely match the lattice spacing of QDs, allowing it to attach to the surface of the perovskite lattice and provide adequate passivation (**Fig. 1b**). Besides, the nucleophilicity of -$OCH_3$, $F^-$, $Cl^-$ and $Br^-$ decreases in turn, according to the calculated electrostatic potential results. Additionally, the triple-attached nucleophilic groups significantly increase their probability of interacting with uncoordinated $Pb^{2+}$.

**Page 5:** The calculated PDOS revealed that the pristine QDs possess imperfect surface sites featuring a conspicuous trap state originating from halide vacancies or uncoordinated $Pb^{2+}$ $6p_z$ orbital (**Fig. 1c**). We then calculated the PDOSs of single-site anchored (TPPO-treated) QDs. The Pb-$6p_z$ trap states around the Fermi level were eliminated entirely by O-2*p*, whereas the uncoordinated $Pb^{2+}$ maintained the trap states. Meanwhile, the trap peaks were separated from the conduction band minimum (CBM) state, showing that the consecutive trap states could not be eliminated sufficiently (**Fig. 1d**). When the TMeOPPO-*p* offered lattice-matched multi-site anchoring interaction, the trap states and the CBM peaks connected completely, revealing that the P=O and -$OCH_3$ groups from TMeOPPO-*p* could strongly interact with uncoordinated $Pb^{2+}$, stabilise the lattice and eliminate the trap states entirely (**Fig. 1e**). Notably, when the difference between the site spacing of groups and perovskite lattice is too large (i.e., TMeOPPO-*o*), enforced coordination will instead introduce substantial strain, leading to severe structural distortion after optimisation—manifested by anomalous phenomena such as the transformation of benzene rings into five-membered rings. In mismatched multi-site models, failure to enforce passivation at every site results in passivation effects analogous to those in single-site models.

**Page 7:** We first compared the average PLQYs of QD solutions treated with different molecules (concentration of 5 mg $mL^{-1}$ in ethyl acetate). The pristine QD and QDs treated with TPPO, TMeOPPO-*o*, TMeOPPO-*p*, TFPPO, TClPPO, and TBrPPO showed average PLQYs of 59%, 70%, 82%, 96%, 92%, 88%, and 87%, respectively (**Fig. 2a** and **Fig. S2**). The QDs treated with TMeOPPO-*p* showed the highest PLQYs, which is consistent with the theoretical calculation results. TMeOPPO-*p* could offer multi-site anchoring interactions and eliminate defects in QDs (**Fig. 2b**), thus designated as the representative molecule for further exploration and labelled as the "target".

**Page 16:** For example, the devices based on the QDs treated with TPPO, TMeOPPO-*o*, TFPPO, TClPPO and TBrPPO achieved the highest radiance of 49,018 mW Sr $m^{-2}$, 54,821 mW Sr $m^{-2}$, 67,410 mW Sr $m^{-2}$, 85,859 mW Sr $m^{-2}$ and 69,587 mW Sr $m^{-2}$, respectively. The maximum EQEs in that order were 19.79%, 20.16%, 23.62%, 22.38% and 21.45%, respectively. For operating stability, we calculated that the values of *n* are 1.87, 1.87, 1.87, 1.86, and 1.86 for the devices based on the TPPO-, TMeOPPO-*o*-, TFPPO-, TClPPO- and TBrPPO-treated QDs, respectively. The $T_{50}$ of the devices in that order could be estimated to be 1,944 h, 3,127 h, 8,307 h, 6,139 h and 4,767 h, respectively.

**Page 17**: Combining the results of theoretical calculation, PLQYs and device performance, we can draw the following conclusions: the site spacing and nucleophilicity of groups are the two key factors that would

affect the performance of QDs. The closer the site spacing is to the perovskite lattice spacing and the stronger nucleophilicity of the groups, the more stable the lattice and fewer defects in QDs can be achieved, thereby facilitating the fabrication of more efficient and stable QLEDs.

**Comment 7:** The labelled number in Fig.S2 is misleading, please check it.

**Response:** We have now updated the figure to avoid confusion (**Fig. R2.9**).

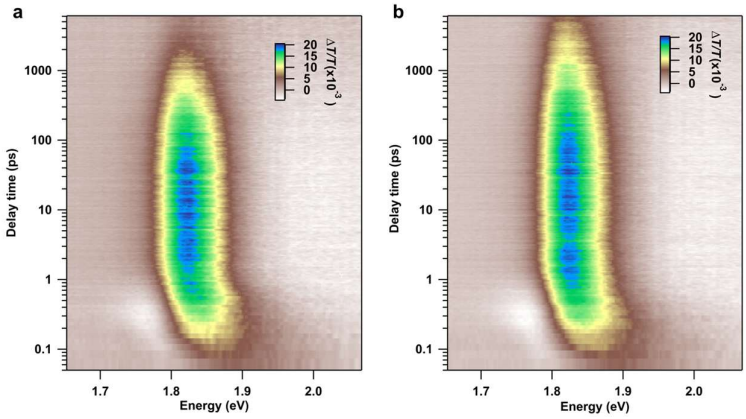


**Fig. R2.9 The ultrafast differential transmission spectra at room temperature. a,** pristine QDs. **b**, target QDs. The photon energy of the pump beam is ~ 2.14 eV. The pump fluence is ~ 0.61uJ/cm$^{-2}$. (**Fig. S3** in the revised Supporting Information)

## Replies to Reviewer #3

**Comments to the Author:**

This study by Zhang and coauthors compare a series of organic molecules, TPPO, TMeOPPO, TFPPO, TClPPO, TBrPPO that can anchor the defect sites in perovskite quantum dots. The authors conduct a series of film and LED device characterisations and conclude that the TMeOPPO offers the best performance among the series. The reason was claimed to be that the TMeOPPO can provide multisite defect anchoring since the distance between the oxygen atoms of the P=O group and the $–OCH_3$ group is 6.5 Å, which matches perfectly with the lattice spacing of $CsPbI_3$ quantum dots (also 6.5 Å). Overall, this is one of the plethora of perovskite surface passivation studies where a good cause-strategy-impact is shown, but a new understanding to the field is much to be desired. While the trend is suggestive, I have a number of concerns including experimental data validation, data interpretation and display. These concerns make it unable for me to recommend publication in Nature Communications. I provide more detailed comments below:

**Comment 1:** The authors pick a series of triphenylphosphine oxides with different substitution groups ($-OCH_3$, -F, -Cl, -Br), and thus different interatomic distance (the authors' word) between the substitution group and the P=O group in the framework. However, there are other variables, primarily the interaction between the substitution groups with un-coordinated $Pb^{2+}$. Clearly, the $–OCH_3$ group has stronger passivation effects on perovskites than the rest of groups. If the trend is indeed due to the ability of a single molecule to anchor two sites due to perfectly-matched (both 6.5 Å) interatomic distance of the passivator with the lattice spacing of $CsPbI_3$ perovskite, and not, for instance, due to the presence of optimal $-OCH_3$ group, the authors will need to conduct reference experiments to rule it out. Overall, I feel that the authors need to compare more than a single series to validate their claim, rather than simply found a specific series where the $–OCH_3$ substituted passivator work better.

**Response:** Thank you for your suggestions. To study the effects of triphenylphosphine oxides with different substitution groups on QDs, we have now synthesised ortho-methoxy-substituted TMePPO (TMeOPPO-*o*) and divided all six molecules (TPPO, TMeOPPO-*o*, TMeOPPO-*p*, TFPPO, TClPPO, and TBrPPO) into three types: single-site (TPPO), lattice-mismatched multi-site (TMeOPPO-*o*, TClPPO and TBrPPO) and lattice-matched multi-site (TMeOPPO-*p* and TFPPO).

First, we calculated the ESP of TPPO, TMeOPPO-*o*, TMeOPPO-*p*, TFPPO, TClPPO, and TBrPPO (**Fig. R3.1**). The -$OCH_3$ group has stronger nucleophilicity than halogen groups. The nucleophilicities of -F, -Cl and -Br decrease successively. The site spacing TFPPO and TMeOPPO-*p* are both very close to the lattice spacing of the perovskite, regarded as lattice-matched multi-site anchoring molecules. TPPO is regarded as single-site molecule, while TMeOPPO-*o*, TClPPO, and TBrPPO are regarded as lattice-mismatched multi-site anchoring molecules.

We then calculated the projected density of states (PDOSs) of pristine QDs, QDs treated by the single-site molecule (TPPO) and QDs treated by the lattice-matched multi-site molecule (TMeOPPO-*p*) (**Fig. R3.1** and **Fig. R3.2**). Notably, we also calculated the PDOSs of QDs treated by the lattice-mismatched multi-site molecule (TMeOPPO-*o*). However, if the difference between the site spacing of groups and the perovskite lattice is too large, forced coordination will instead damage the lattice structure. The theoretical calculation results reveal that only the lattice-matched multi-site anchoring interaction can eliminate the trap states entirely.

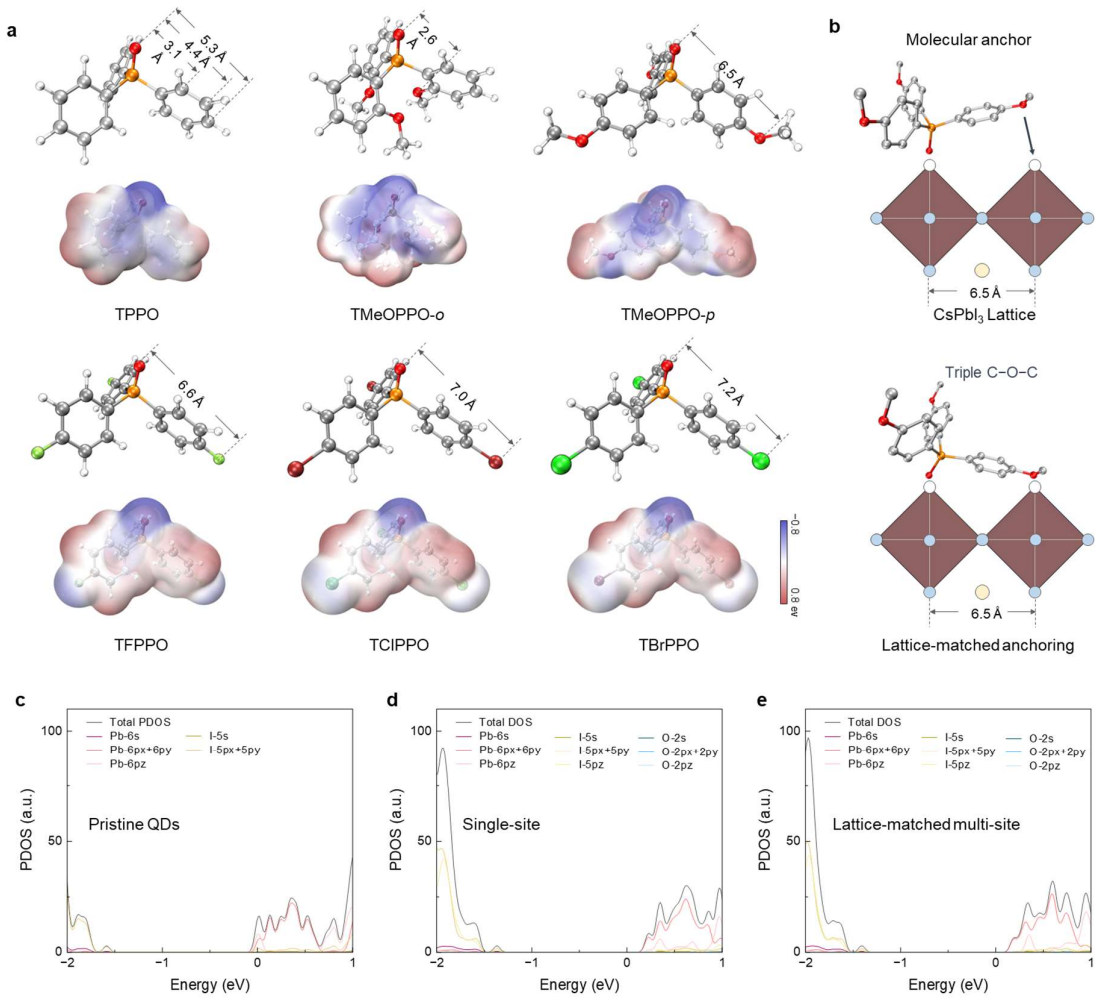

**Fig. R3.1 Lattice-matched multi-site-anchoring strategy. a**, Schematic illustration of lattice-matched anchoring molecule design. **b**, Schematic illustration of the lattice-matched molecular anchoring effect. **c**, PDOS of the perovskite QDs with surface defects. **d**, PDOS of the perovskite QDs treated with single-site molecule. **e**, PDOS of the perovskite QDs with multi-site lattice-matched anchoring effect. (**Fig. 1** in the revised manuscript)

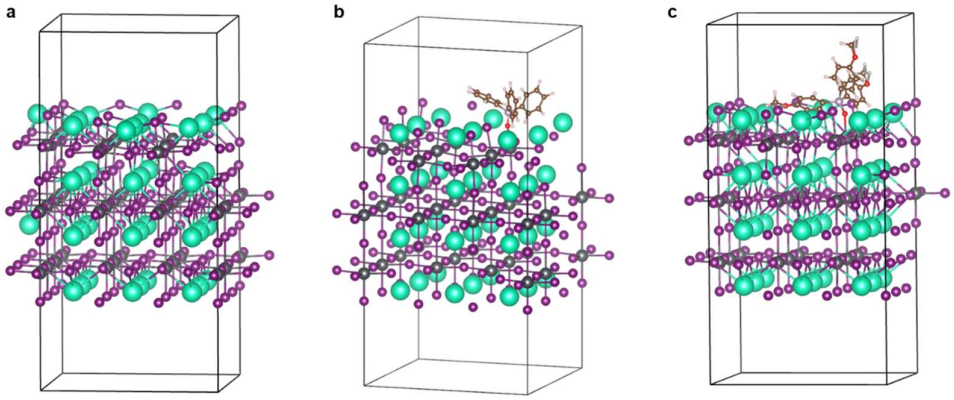


**Fig. R3.2 Crystal models of $CsPbI_3$ for DFT calculation. a**, $CsPbI_3$ with trap defects. **b**, $CsPbI_3$ treated with single-site molecule. **c**, $CsPbI_3$ with lattice-matched multi-site anchoring effect. (**Fig. S1** in the revised Supporting Information)

Lastly, we compared the average PLQYs of QD solutions (**Fig. R3.3** and **Fig. R3.4**) and their EL performance treated with different molecules (**Fig. R3.5**). We summarised all these data in **Table R3.1**.

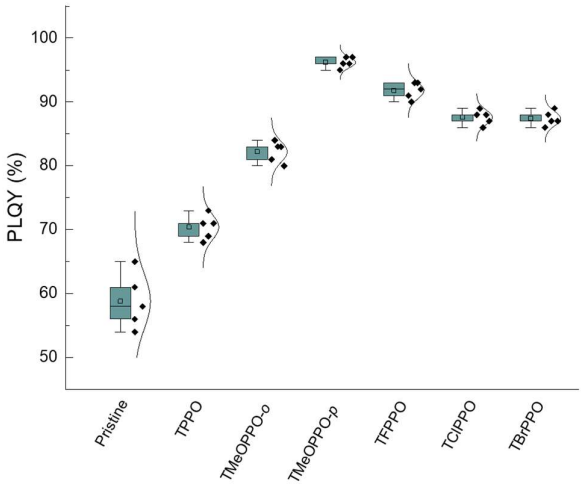


**Fig. R3.3** PLQYs of QD solution treated by different molecules. (**Fig. S2** in the revised Supporting Information)

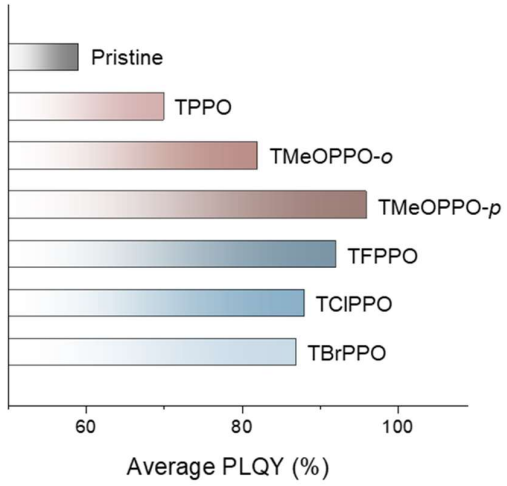


**Fig. R3.4** Average PLQYs of QD solution treated by different molecules. (**Fig. 2a** in the revised manuscript.)

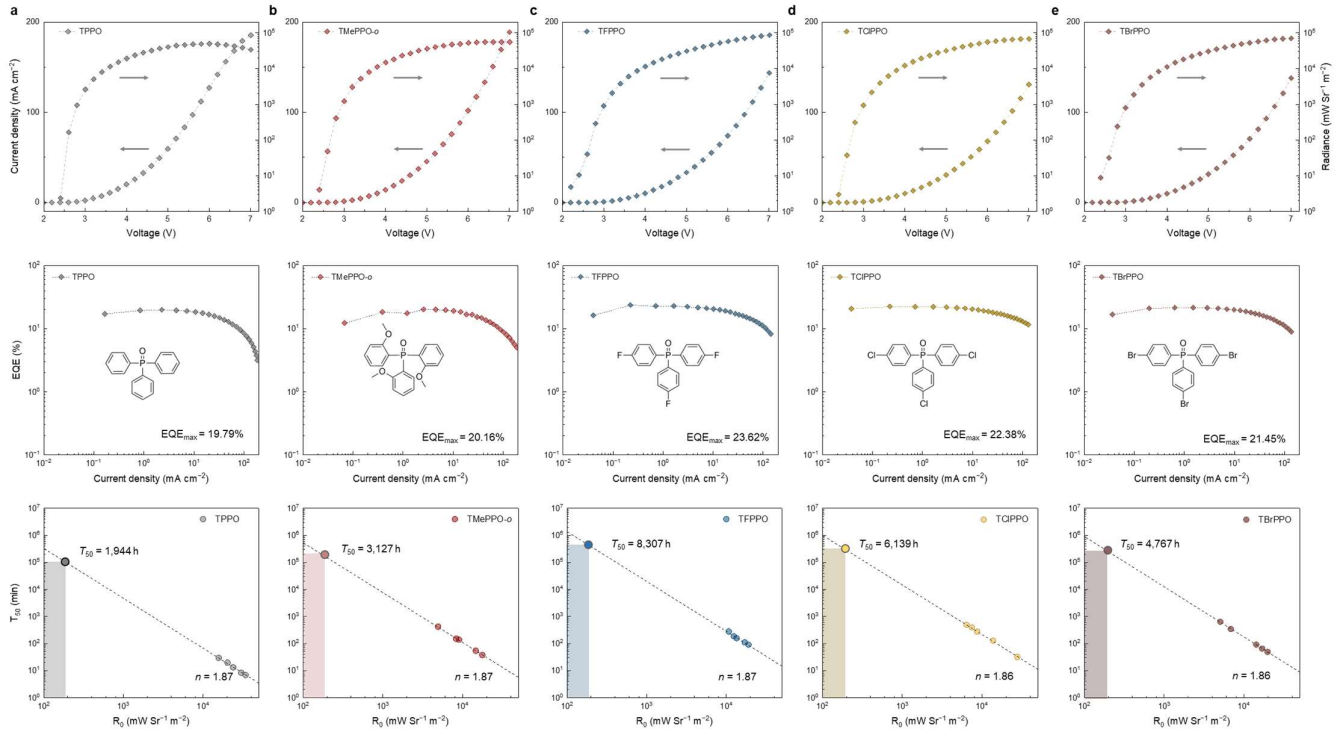


**Fig. R3.5 Performance of QLEDs by using various designed molecules.** Electro-optical conversion performance and stability of QLEDs by using various designed molecules, containing current density-radiance-voltage curve, EQE curve (the insert is the chemical structure) and operating stability. **a**, TPPO. **b**, TMeOPPO-*p*. **c**, TFPPO. **d**, TClPPO. **e**, TBrPPO (**Fig. 6** in the revised manuscript)

**Table R3.1** Device performance of QLEDs with different molecules (**Table 1** in the revised manuscript)

| Device | Type | | Radiance (mW $Sr^{-1}$ $m^{-2}$ ) | $EQE_{max}$ (%) | $EQE_{average}$ (%) | $T_{50}$* (h) |
|---|---|---|---|---|---|---|
| Control | / | / | 42,809 @6.8 V | 15.14 | 12.8 | 1,350 |
| TPPO | Single-site | / | 49,018 @6.0 V | 19.79 | 17.7 | 1,944 |
| TMeOPPO-*o* | Multi-site | Lattice-mismatched | 54,821 @7.0 V | 20.16 | 19.4 | 3,127 |
| TMeOPPO-*p* | Multi-site | Lattice-matched | 119,037 @6.8 V | 26.91 | 25.3 | 23,420 |
| TFPPO | Multi-site | Lattice-matched | 67,410 @7.0 V | 23.62 | 21.8 | 8,307 |
| TClPPO | Multi-site | Lattice-mismatched | 85,859 @7.0 V | 22.38 | 20.3 | 6,139 |
| TBrPPO | Multi-site | Lattice-mismatched | 69,587 @7.0 V | 21.45 | 19.6 | 4,767 |

*For initial radiance of 190 mW $sr^{-1}$ $m^{-2}$, equivalent to a luminance of 100 cd $m^{-2}$ for green perovskite LEDs.

According to the theoretical and experimental evidence above, we have reached the following conclusions: (i) All these molecules can improve the performance of QDs, which can be attributed to the fact that these groups (P=O, halogens, and -$OCH_3$) can interact strongly with uncoordinated $Pb^{2+}$ through electron-donating effects. (ii) The nucleophilicity of the group is a key factor. TMeOPPO-*p*-treated QDs showed better optical and electrical properties than TFPPO-treated QDs, indicating that the stronger nucleophilicity of the groups enables a better multi-site anchoring effect. (iii) The site spacing is another key factor that affects the performance of QDs and QLEDs. The optical and electrical properties of TMeOPPO-*o*-treated QDs are not as good as those of TFPPO-treated QDs, let alone TMeOPPO-*p*-treated QDs, indicating that a suitable site spacing is also important.

In sum, the closer the site spacing is to the perovskite lattice spacing and the stronger nucleophilicity of the groups, the more stable the lattice and fewer defects in QDs can be achieved, thereby facilitating the fabrication of more efficient and stable QLEDs.

We have now added the corresponding contents and updated the corresponding figures and table as follows:

**Page 5:** In order to study the effect of site spacing and nucleophilicity on QDs, we synthesised a series of multi-site anchoring molecules, including TMeOPPO-*o*, TMeOPPO-*p*, TFPPO, TClPPO, and TBrPPO (**Fig. 1a**). The site spacing of multi-site anchoring molecules in that order is 2.6 Å, 6.5 Å, 6.6 Å, 7.0 Å and 7.2 Å, respectively. The TMeOPPO-*p* could precisely match the lattice spacing of QDs, allowing it to attach to the surface of the perovskite lattice and provide adequate passivation (**Fig. 1b**). Besides, the nucleophilicity of -$OCH_3$, $F^-$, $Cl^-$ and $Br^-$ decreases in turn, according to the calculated electrostatic potential results. Additionally, the triple-attached nucleophilic groups significantly increase their probability of interacting with uncoordinated $Pb^{2+}$.

**Page 5:** The calculated PDOS revealed that the pristine QDs possess imperfect surface sites featuring a conspicuous trap state originating from halide vacancies or uncoordinated $Pb^{2+}$ $6p_z$ orbital (**Fig. 1c**). We then calculated the PDOSs of single-site anchored (TPPO-treated) QDs. The Pb-$6p_z$ trap states around the Fermi level were eliminated entirely by O-2*p*, whereas the uncoordinated $Pb^{2+}$ maintained the trap states. Meanwhile, the trap peaks were separated from the conduction band minimum (CBM) state, showing that the consecutive trap states could not be eliminated sufficiently (**Fig. 1d**). When the TMeOPPO-*p* offered lattice-matched multi-site anchoring interaction, the trap states and the CBM peaks connected completely, revealing that the P=O and -$OCH_3$ groups from TMeOPPO-*p* could strongly interact with uncoordinated $Pb^{2+}$, stabilise the lattice and eliminate the trap states entirely (**Fig. 1e**). Notably, when the difference between the site spacing of groups and perovskite lattice is too large (i.e., TMeOPPO-*o*), enforced coordination will instead introduce substantial strain, leading to severe structural distortion after optimisation—manifested by anomalous phenomena such as the transformation of benzene rings into five-membered rings. In mismatched multi-site models, failure to enforce passivation at every site results in passivation effects analogous to those in single-site models.

**Page 7:** We first compared the average PLQYs of QD solutions treated with different molecules (concentration of 5 mg $mL^{-1}$ in ethyl acetate). The pristine QD and QDs treated with TPPO, TMeOPPO-*o*, TMeOPPO-*p*, TFPPO, TClPPO, and TBrPPO showed average PLQYs of 59%, 70%, 82%, 96%, 92%, 88%, and 87%, respectively (**Fig. 2a** and **Fig. S2**). The QDs treated with TMeOPPO-*p* showed the highest PLQYs, which is consistent with the theoretical calculation results. TMeOPPO-*p* could offer multi-site anchoring interactions and eliminate defects in QDs (**Fig. 2b**), thus designated as the representative molecule for further exploration and labelled as the "target".

**Page 16:** For example, the devices based on the QDs treated with TPPO, TMeOPPO-*o*, TFPPO, TClPPO

and TBrPPO achieved the highest radiance of 49,018 mW Sr $m^{-2}$, 54,821 mW Sr $m^{-2}$, 67,410 mW Sr $m^{-2}$, 85,859 mW Sr $m^{-2}$ and 69,587 mW Sr $m^{-2}$, respectively. The maximum EQEs in that order were 19.79%, 20.16%, 23.62%, 22.38% and 21.45%, respectively. For operating stability, we calculated that the values of *n* are 1.87, 1.87, 1.87, 1.86, and 1.86 for the devices based on the TPPO-, TMeOPPO-*o*-, TFPPO-, TClPPO- and TBrPPO-treated QDs, respectively. The $T_{50}$ of the devices in that order could be estimated to be 1,944 h, 3,127 h, 8,307 h, 6,139 h and 4,767 h, respectively.

**Page 17**: Combining the results of theoretical calculation, PLQYs and device performance, we can draw the following conclusions: the site spacing and nucleophilicity of groups are the two key factors that would affect the performance of QDs. The closer the site spacing is to the perovskite lattice spacing and the stronger nucleophilicity of the groups, the more stable the lattice and fewer defects in QDs can be achieved, thereby facilitating the fabrication of more efficient and stable QLEDs.

**Comment 2:** Here, the authors report improved "EQE of up to 27%" and "peak luminance of ~ 10^3 cd/$cm^2$ (Fig. S5), and operating half-life of over 23000 h".

i. These improvements appear real vs an internal control. However, the device performance, particularly luminance, still remain clearly inferior to existing perovskite QLEDs reports in the literature as summarised in Xiong et al., Nature, 2024, 633, 344-350. Can the authors comment on this, and maybe consider/discuss mitigation strategies to address this? Meanwhile, can the authors plot EQE-Luminance for direct comparison?

**Response:** Luminance (*L*) is a perception-based measure of apparent brightness, while Radiance (*R* or $L_e$) is a physical measure of electromagnetic radiation intensity, independent of human vision. Luminance measures the luminous intensity of light per unit area in a specific direction, taking into account the human eye's sensitivity to different wavelengths of light. It reflects how "bright" a light source or object appears to the human observer. Radiance measures the radiant power (energy per unit time) emitted, reflected, or transmitted by a surface per unit area in a specific direction, without considering human visual perception. It is a physical quantity that describes the distribution of electromagnetic radiation (including all wavelengths).

There is the following relationship between Luminance and Radiance:

$$L = \frac{1}{K_m} \int R(\lambda)\ V(\lambda)\ d\lambda$$

Where $K_m$ is a constant, representing the maximum spectral luminous efficacy ($K_m$ = 683 lm $W^{-1}$ for

monochromatic light at 555 nm). The value of $V(\lambda=542\ nm)$ is 0.966 (Xiong *et al.* reported a green perovskite LED, not a perovskite QLED actually, located at 542 nm), which is almost 150 times that of $V(\lambda=693\ nm)$, as shown in **Fig.R3.6**. Thus, $L(\lambda=542\ nm)$ is much higher than $L(\lambda=693\ nm)$. In simple terms, 1 cd $m^{-2}$ at 693 nm is equivalent to 150 cd $m^{-2}$ at 542 nm. Thus, the luminance of reported green perovskite QLED is much higher than reported blue and red QLED.

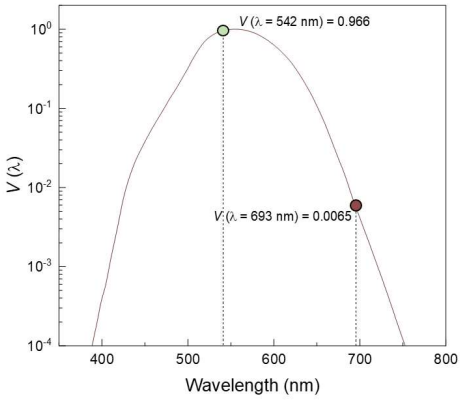


**Fig. R3.6** Human visual efficiency function as wavelength (380~750 nm).

Besides, deep-red LEDs are more widely applied in the field of precise biomedical treatment or biological lighting than in displays. Thus, to more accurately evaluate the operating stability of deep-red QLEDs, in this work, we chose radiance, which is used in precise biomedical treatment or biological lighting, rather than luminance, which is commonly used in green or pure red emission.

We have now updated the summary of the reported perovskite QLED characteristics (600~800 nm) in **Table S3.2**. The luminance of reported pure-red (600-660 nm) QLEDs ranges from $10^3$ to $10^4$ cd $m^{-2}$. The luminance of reported deep-red (660-750 nm) QLEDs ranges from $10^2$ to $10^3$ cd $m^{-2}$. We can find that our work exhibited the highest luminance among all deep-red QLEDs (660~750 nm) and the highest radiance among all QLEDs (600~800 nm). As suggested, we have now provided luminance-EQE curves and radiance-EQE curves of the control and target QLEDs in **Fig. R3.7**.

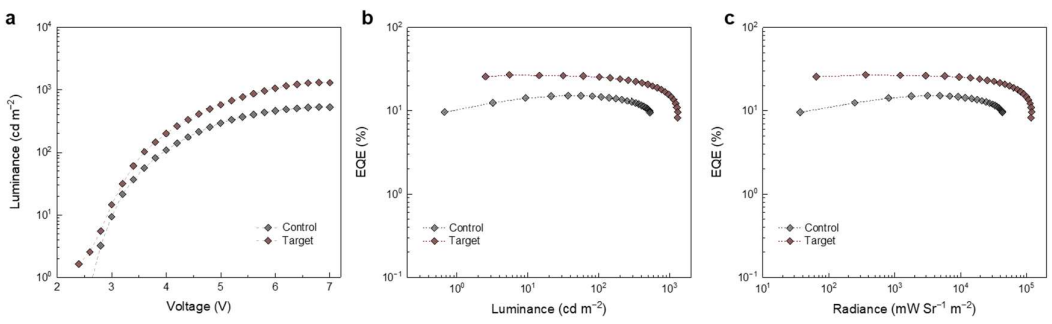

**Fig. R3.7 EL performance of the control and target QLEDs. a**, Luminance-voltage curves. **b**, Luminance-EQE curves. **c**, Radiance-EQE curves. (**Fig. S6** in Supporting Information)

**Table R 3.2** Summary of the typical reported perovskite QLEDs (600~800 nm).

| QD | EL Peak (nm) | EQE (%) | $L_{max}/R_{max}$ (cd $m^{-2}$/mW $sr^{-1}$ $m^{-2}$) | $T_{50}$ (h) | Condition* | Ref. |
|---|---|---|---|---|---|---|
| $MAPb(Br/I)_3$ | 620 | 20.3 | 627/~1,880 | 2.17<br>0.27 | 1 mA $cm^{-2}$<br>10 mA $cm^{-2}$ | 1 |
| $CsPb(Br/I)_3$ | 635 | 22.8 | 12,910/~77,460 | 1 | 100 cd $m^{-2}$/~600 mW $sr^{-1}$ $m^{-2}$ | 2 |
| $CsPbI_3$ | 636 | ~22.5 | 7,000/~42,000 | ~3,900 | 100 cd $m^{-2}$/~600 mW $sr^{-1}$ $m^{-2}$ | 3 |
| $CsPb(Br/I)_3$ | 637 | 21.8 | 6,471/~38,946 | 1.17 | 100 cd $m^{-2}$/~600 mW $sr^{-1}$ $m^{-2}$ | 4 |
| $CsPb(Cl/I)_3$ | 638 | 26.1 | 2,511/~17,577 | 7.5 | 100 cd $m^{-2}$/~700 mW $sr^{-1}$ $m^{-2}$ | 5 |
| $CsPbI_3$ | 640 | 23 | ~1000/7,700 | 5<br>5.67 | 200 cd $m^{-2}$/~1540 mW $sr^{-1}$ $m^{-2}$<br>0.1 mA $cm^{-2}$ | 6 |
| $CsPbI_3$ | 644 | 28.5 | 4,140/~33,120 | 30.4 | 100 cd $m^{-2}$/~800 mW $sr^{-1}$ $m^{-2}$ | 7 |
| $CsPbI_3$ | 685 | 21.23 | 190/~17,000 | 0.67 | 100 cd $m^{-2}$/~8500 mW $sr^{-1}$ $m^{-2}$ | 8 |
| $CsPbI_3$ | 686 | 26.0 | 492/43,691 | 10,587<br>5.17 | 190 mW $sr^{-1}$ $m^{-2}$<br>13.3 mA $cm^{-2}$ | 9 |
| $FAPbI_3$ | 776 | 22.86 | NA/24,000 | 1.83 | 1000 mW $sr^{-1}$ $m^{-2}$ | 10 |
| $FAPbI_3$ | 780 | 20.79 | NA/29,470 | 1.75 | 1000 mW $sr^{-1}$ $m^{-2}$ | 11 |
| **$CsPbI_3$** | **693** | **26.91** | **1,305/119,037** | **23,420**<br>**7.43** | **190 mW $sr^{-1}$ $m^{-2}$**<br>**10 mA $cm^{-2}$** | **This work** |

*Radiance is estimated by testing as-fabricated perovskite QLED with corresponding EL peak.

ii. Since half lifetime of LED is dependent on the current density and the initial luminance, and considering

that the long life-time is one main claim of this manuscript, to ensure fair and direct comparison, I would recommend the authors to either follow the suggested test protocols (both 100 and 1000 cd/m2) as suggested by Woo et al., Nat. Photon., 2021, 15, 630 – 634, or plot the half lifetime of fabricated LEDs against current density and compare that with the LED half lifetime summary by Zhao et al., Matter, 2024, 7, 772-793.

**Response:** For EL performance, we have now listed EQE, luminance and radiance. For operating stability, we have now listed the test conditions, including current density, luminance and equivalent radiance. As can be seen in **Fig. R3.8** and **Table R3.2**, our work is quite competitive in the aspects of EQE, luminance/ radiance and operating stability. For our deep-red QLED, 100 cd $m^{-2}$ at 693 nm is equivalent to ~9000 mW $sr^{-1}$ $m^{-2}$, hence $T_{50}$ ($L_0$ = 100 cd $m^{-2}$) is ~1200 min (**Fig. R3.8c**). The $T_{50}$ is 446 min under a constant current density of 10 mA $cm^{-2}$ (**Fig. R3.8d**).

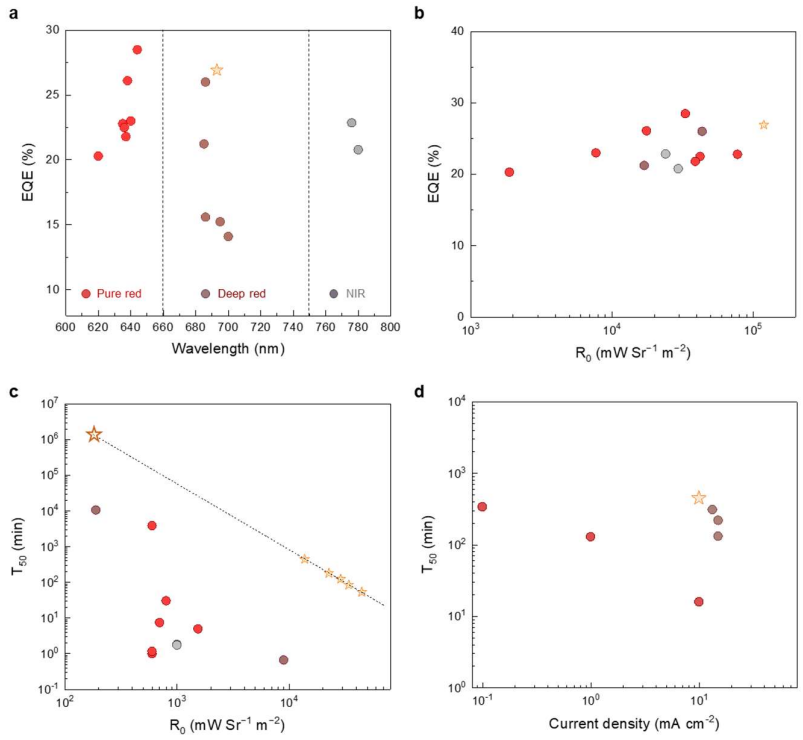


**Fig. R3.8 Summary of the reported iodine-based perovskite QLED characteristics (600~800 nm).** (**Fig. S11** in Supporting Information)

iii. Statistics are very important for comparing device performance, the authors should report statistics rather than single value, especially in Table 1.

**Response:** We have now reported statistics in QLED performance and updated **Table 1** (**Table R3.3**).

**Table R3.3** Device performance of QLEDs with different molecules (**Table 1** in the revised manuscript)

| Device | Type | | Radiance (mW $Sr^{-1}$ $m^{-2}$ ) | $EQE_{max}$ (%) | $EQE_{average}$ (%) | $T_{50}$* (h) |
|---|---|---|---|---|---|---|
| Control | / | / | 42,809 @6.8 V | 15.14 | 12.8 | 1,350 |
| TPPO | Single-site | / | 49,018 @6.0 V | 19.79 | 17.7 | 1,944 |
| TMeOPPO-*o* | Multi-site | Lattice-mismatched | 54,821 @7.0 V | 20.16 | 19.4 | 3,127 |
| TMeOPPO-*p* | Multi-site | Lattice-matched | 119,037 @6.8 V | 26.91 | 25.3 | 23,420 |
| TFPPO | Multi-site | Lattice-matched | 67,410 @7.0 V | 23.62 | 21.8 | 8,307 |
| TClPPO | Multi-site | Lattice-mismatched | 85,859 @7.0 V | 22.38 | 20.3 | 6,139 |
| TBrPPO | Multi-site | Lattice-mismatched | 69,587 @7.0 V | 21.45 | 19.6 | 4,767 |

*For initial radiance of 190 mW $sr^{-1}$ $m^{-2}$, equivalent to a luminance of 100 cd $m^{-2}$ for green perovskite LEDs.

Reference:


1 Hassan, Y. *et al.* Ligand-engineered bandgap stability in mixed-halide perovskite LEDs. *Nature* **591**, 72-77 (2021).

2 Zhang, J. *et al.* Ligand-Induced Cation–π Interactions Enable High-Efficiency, Bright, and Spectrally Stable Rec. 2020 Pure-Red Perovskite Light-Emitting Diodes. *Adv. Mater.* **35** (2023).

3 Wang, Y. K. *et al.* Long-range order enabled stability in quantum dot light-emitting diodes. *Nature* (2024).

4 Xie, M. *et al.* Suppressing Ion Migration of Mixed-Halide Perovskite Quantum Dots for High Efficiency Pure-Red Light-Emitting Diodes. *Adv. Funct. Mater.* (2023).

5 Feng, Y. *et al.* Nucleophilic Reaction-Enabled Chloride Modification on CsPbI3 Quantum Dots for Pure Red Light-Emitting Diodes with Efficiency Exceeding 26 %. *Angew. Chem. Int. Ed.* **63**, e202318777 (2024).

6 Wang, Y. K. *et al.* All-Inorganic Quantum-Dot LEDs Based on a Phase-Stabilised alpha-CsPbI(3) Perovskite. *Angew. Chem. Int. Ed.* **60**, 16164-16170 (2021).

7 Li, H. *et al.* Nanosurface-reconstructed perovskite for highly efficient and stable active-matrix light-emitting diode display. *Nat. Nanotechnol.* **19**, 638-645 (2024).

8 Cheng, H. *et al.* Size Enlargement of CsPbI3 Perovskite Nanocrystals by Trioctylphosphine in the Synthesis for Highly Efficient Deep-Red Light-Emitting Diodes. *Adv. Electron. Mater.*, 2400334 (2024).

9 Chen, J. *et al.* Molecule-induced ripening control in perovskite quantum dots for efficient and stable light-emitting diodes. *Sci. Adv.*, eado7159 (2025).

10 Liu, Z. S. *et al.* Liquid bidentate ligand for full ligand coverage towards efficient near-infrared perovskite quantum dot LEDs. *Light: Science & Applications* **14**, 35 (2025).

11 Wang, Y. *et al.* Ligand-Solvent Coordination Enables Comprehensive Trap Passivation for Efficient Near-

**Comment 3:** Overall, the manuscript would benefit from more discussion of the results, and what was learnt, rather than simply stating what the results were. As an example, in Figure 6, the authors simply introduced the radiance, EQE and T50 data of LEDs treated with TFPPO, TClPPO and TBrPPO, without discussing possible reasons causing the difference.

**Response:** By adding the data of TPPO- and TMeOPPO-*o* treated QDs and QLEDs (**Fig. R3.9** and **Table R3.4**), combined with our updated theoretical calculation results, we have now summarised the regularity and revealed new mechanisms. We can draw the following conclusions: the site spacing and nucleophilicity of groups are the two key factors that affect the performance of QDs and QLEDs. The closer the site spacing is to the perovskite lattice spacing and the stronger nucleophilicity of the groups, the more stable the lattice and fewer defects in QDs can be achieved, thereby facilitating the fabrication of more efficient and stable QLEDs.

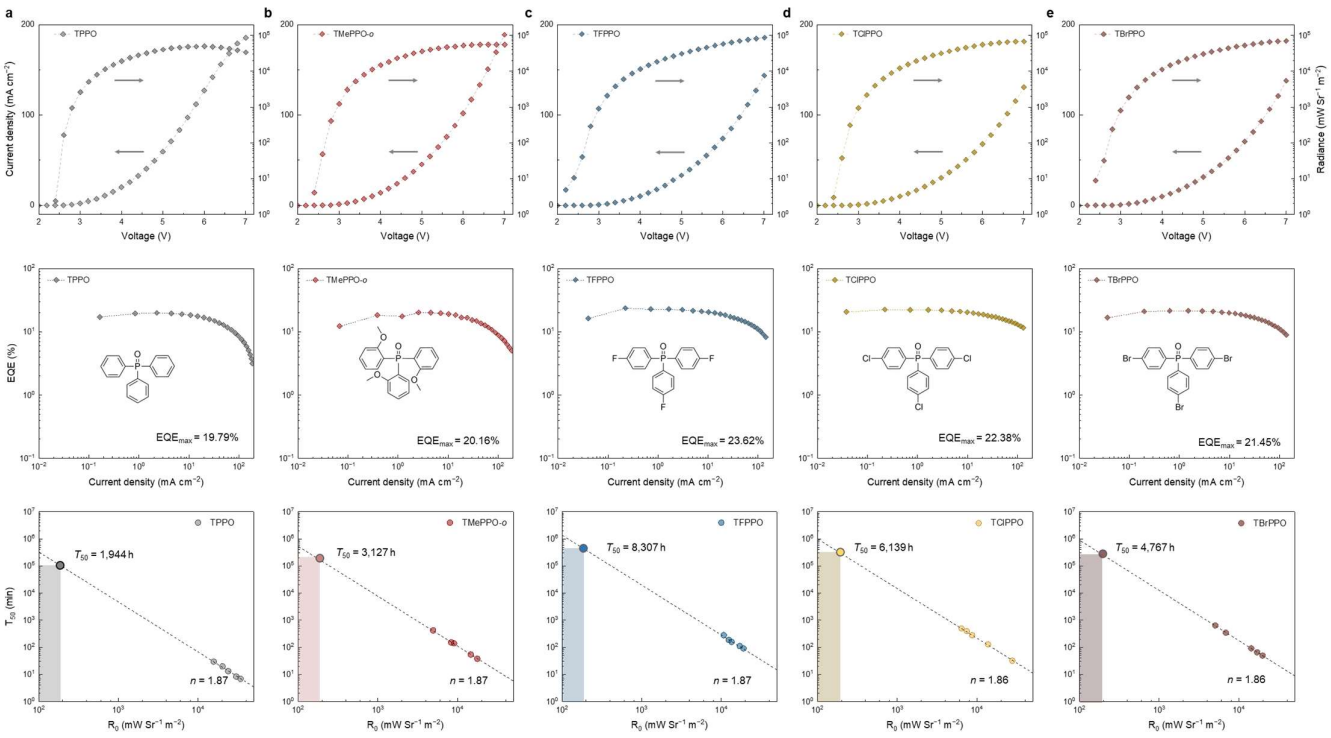


**Fig. R3.9 Performance of QLEDs by using various designed molecules.** Electro-optical conversion performance and stability of QLEDs by using various designed molecules, containing current density-radiance-voltage curve, EQE curve (the insert is the chemical structure) and operating stability. **a**, TPPO. **b**, TMeOPPO-*p*. **c**, TFPPO. **d**, TClPPO. **e**, TBrPPO (**Fig. 6** in the revised manuscript)

We have now added the corresponding contents and updated the corresponding figures and table as follows:

**Page 16:** For example, the devices based on the QDs treated with TPPO, TMeOPPO-*o*, TFPPO, TClPPO and TBrPPO achieved the highest radiance of 49,018 mW Sr $m^{-2}$, 54,821 mW Sr $m^{-2}$, 67,410 mW Sr $m^{-2}$, 85,859 mW Sr $m^{-2}$ and 69,587 mW Sr $m^{-2}$, respectively. The maximum EQEs in that order were 19.79%, 20.16%, 23.62%, 22.38% and 21.45%, respectively. For operating stability, we calculated that the values of *n* are 1.87, 1.87, 1.87, 1.86, and 1.86 for the devices based on the TPPO-, TMeOPPO-*o*-, TFPPO-, TClPPO- and TBrPPO-treated QDs, respectively. The $T_{50}$ of the devices in that order could be estimated to be 1,944 h, 3,127 h, 8,307 h, 6,139 h and 4,767 h, respectively.

**Page 17**: Combining the results of theoretical calculation, PLQYs and device performance, we can draw the following conclusions: the site spacing and nucleophilicity of groups are the two key factors that would affect the performance of QDs. The closer the site spacing is to the perovskite lattice spacing and the stronger nucleophilicity of the groups, the more stable the lattice and fewer defects in QDs can be achieved, thereby facilitating the fabrication of more efficient and stable QLEDs.

**Table R3.4** Device performance of QLEDs with different molecules (**Table 1** in the revised manuscript)

| Device | Type | | Radiance (mW $Sr^{-1}$ $m^{-2}$) | $EQE_{max}$ (%) | $EQE_{average}$ (%) | $T_{50}$* (h) |
|---|---|---|---|---|---|---|
| Control | / | / | 42,809 @6.8 V | 15.14 | 12.8 | 1,350 |
| TPPO | Single-site | / | 49,018 @6.0 V | 19.79 | 17.7 | 1,944 |
| TMeOPPO-*o* | Multi-site | Lattice-mismatched | 54,821 @7.0 V | 20.16 | 19.4 | 3,127 |
| TMeOPPO-*p* | Multi-site | Lattice-matched | 119,037 @6.8 V | 26.91 | 25.3 | 23,420 |
| TFPPO | Multi-site | Lattice-matched | 67,410 @7.0 V | 23.62 | 21.8 | 8,307 |
| TClPPO | Multi-site | Lattice-mismatched | 85,859 @7.0 V | 22.38 | 20.3 | 6,139 |
| TBrPPO | Multi-site | Lattice-mismatched | 69,587 @7.0 V | 21.45 | 19.6 | 4,767 |

*For initial radiance of 190 mW $sr^{-1}$ $m^{-2}$, equivalent to a luminance of 100 cd $m^{-2}$ for green perovskite LEDs.

**Comment 4:** In the energy level diagram shown in Figure 4c, the schematic appears to place the LUMO of PEDOT:PSS:PFI below –5.5 eV, and indicate that holes are injected from the ITO into the LUMO of PEDOT:PSS:PFI, which is conceptually incorrect and misleading. How do the authors determine the energy levels of PEDOT:PSS:PFI? If the authors intended to depict the work function instead of the LUMO/HOMO levels, the figure should be revised to reflect this distinction clearly.

**Response:** The energy level of PEDOT: PSS: PFI was drawn referencing another report (**Fig. R3.10**). To avoid misunderstanding, we redrawn the energy level diagram shown in **Fig. 3d** and **Fig. 4c**.

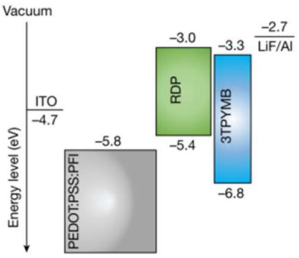


**Fig. R3.10.** Energy band diagram of perovskite LED, which is taken from *Nature, 599, 594 (2021).*

We have now updated the corresponding figures as follows:

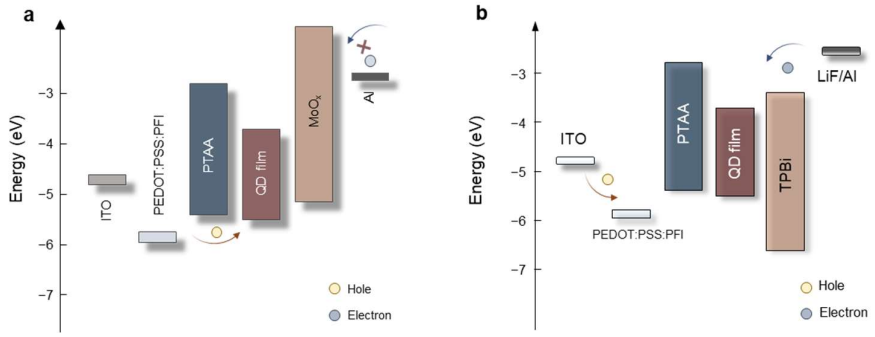


**Fig. R3.11. a**, Energy diagram of the hole-only devices (**Fig.3d** in the revised manuscript). **b**, Energy diagram of the QLED (**Fig.4c** in the revised manuscript).

**Comment 5:** There are lots of discrepancies in the presented experimental data. For example, the authors report that in their QLED device, the PEDOT:PSS:PFI layer is 180 nm thick, the PTAA layer is 40 nm, the perovskite QD layer is 30 nm, and the TPBi layer is 40 nm. Several concerns arise from these claims:

i. What is the rationale for using an HTL with a total thickness of approximately 220 nm? Such a thick HTL is likely to introduce significant series resistance, potentially hindering hole injection efficiency.

**Response:** We followed other reports to fabricate PEDOT: PSS: PFI layer (**Fig. R3.12**, *Nature, 599, 594 (2021); Nat. Nanotechnol. 19, 638 (2024)*). The thickness of the reported HTL layers is ~210 nm. The injection of electrons and holes into the light-emitting layer should be balanced for higher EQE and better stability. The thickness and spin coating parameters of each functional layer have all been optimised before for the best performance.

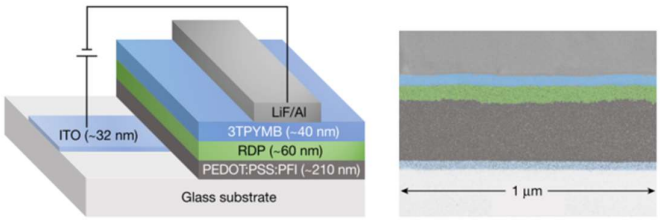


**Fig. R3.12.** Device structure and cross-sectional TEM image, which is taken from *Nature, 599, 594 (2021).*

We also tried the architecture of ITO/ PEDOT: PSS / PTAA / QD film / TPBi / LiF / Al and ITO/ PEDOT: PSS: PFI / QD film / TPBi / LiF / Al before. The device with an ITO/ PEDOT: PSS: PFI / PTAA / QD film / TPBi / LiF / Al architecture showed the best performance (**Fig. R3.13**). They showed maximum EQEs of 18.94% with a big efficiency roll-off and 1.97%, respectively. By contrast, the target QLED showed a maximum EQE of 27% with a small efficiency roll-off, indicating that its functional layers matched well with each other, which ensures balanced carrier transport and injection.

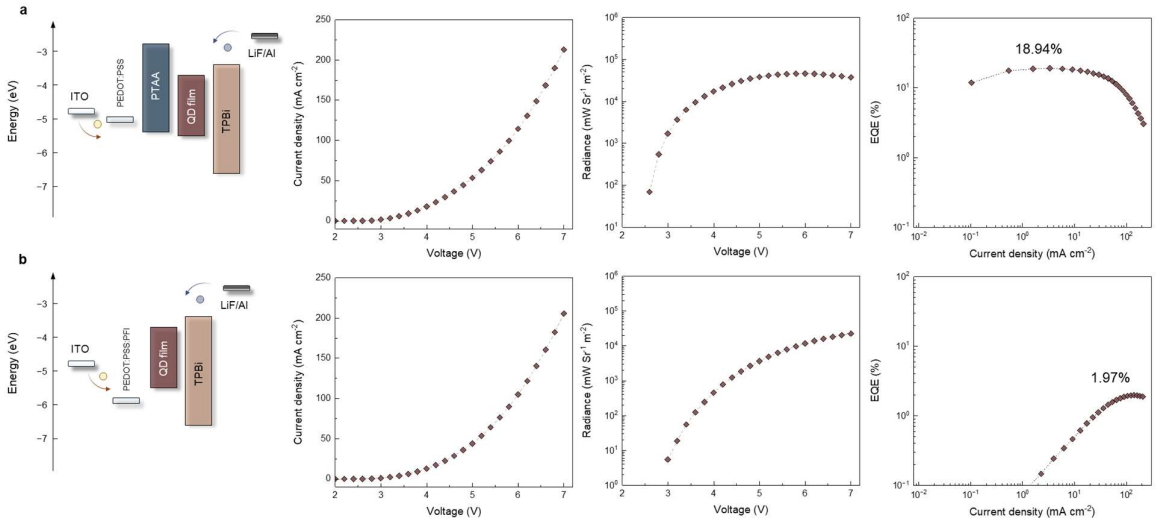


**Fig. R3.13 a**, Energy diagram of the hole-only devices (**Fig.3d** in the revised manuscript). **b**, Energy diagram of the QLED

ii. The reported film thicknesses are counterintuitive based on the stated fabrication conditions. Specifically, spin-coating PEDOT:PSS at 4000 rpm for 45 seconds would not typically yield a film as thick as 180 nm. Similarly, a 5 mg/mL PTAA solution spin-coated 4000 rpm for 45 seconds would not be expected to result in a 40 nm film. How were these thicknesses determined? The authors should provide measurement data to substantiate these values.

**Response:** We mixed Nafion perfluorinated resin solution (PFI, tetrafluoroethylene-perfluoro-3, 6-dioxa-4-methyl-7-octenesulfonic acid copolymer) with PEDOT: PSS at a mass ratio of 1:1 to regulate the energy level of HTL. We spin-coated the mixture onto the ITO-coated glass substrates at 4000 r.p.m. for 45 s, followed by annealing at 150 ℃ for 30 min in the atmosphere. The PFI is a polymer with relatively high viscosity. Thus, spin-coating PEDOT:PSS: PFI would yield a film much thicker than spin-coating PEDOT: PSS directly and affect the thickness of the PTAA layer subsequently. Meanwhile, the thickness of PEDOT: PSS: PFI layer is consistent with other reports. We have now provided the original cross-sectional SEM image of the QLED to confirm the thickness of the PEDOT: PSS: PFI and PTAA layers.

iii. The reported film thicknesses also appear inconsistent with the SEM cross-sectional image in Figure 4b. The scale bar is not labeled, making interpretation difficult; however, visually, the PTAA layer appears roughly three times thicker than the TPBi layer, despite both being reported as 40 nm. Moreover, PTAA also seems approximately three times thicker than the ITO layer, which is also not expected. These discrepancies raise concerns about the accuracy of the layer assignments in the SEM image.

**Response:** We are sorry for the typo and the missing scale bar. The scale bar is 200 nm, and the thickness of PTAA is ~90 nm, as shown in the original cross-sectional SEM image below (**Fig. R3.14**). We have now corrected the caption and relevant content.

**Page 12**: Based on these high-quality perovskite QD films, we fabricated QLEDs with an ITO/ PEDOT: PSS: PFI (180 nm)/ PTAA (90 nm)/ QD film (30 nm)/ 1,3,5-tris(1-phenyl-1H-benzimidazol-2-yl)benzene (TPBi, 40 nm)/ LiF (1 nm)/ Al (100 nm) architecture (**Fig. 4a-c**).

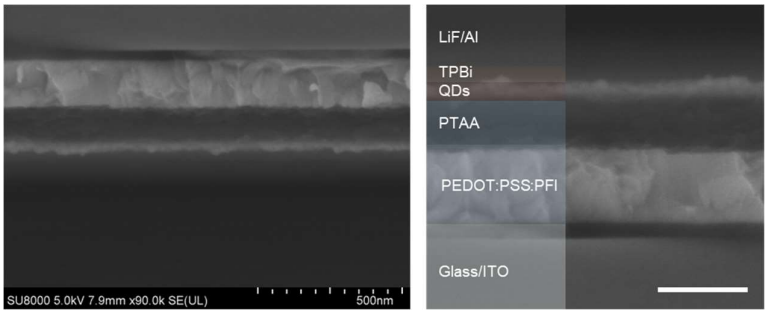


**Fig. R3.14** The original cross-sectional SEM image of the QLED (left) and the cross-sectional SEM image of the QLED. Scale bar, 200 nm (right, **Fig.4b** in the revised manuscript).

**Comment 6:** Missing critical experimental details: the manuscript omits lots of experimental details which are crucial for understanding the actions and ensuring reproducibility. For instance:

i. The authors simply stated "For the target QDs, TMePPO in ethyl acetate was added during the purification process". What is the concentration of TMePPO solution? What is the volume ratio of TMePPO solution relative to the QD solution? Has the TMePPO replaced the ligands (OA, OAm)? This might explain the size changes in STEM images in Figure 2b? These information is vital for elucidating the role of TMePPO in surface treatment and should be clearly stated.

**Response:** We have now provided the details of the molecule concentration in the Supporting Information. For treated QDs, different molecules (TPPO, TMeOPPO-*o*, TMeOPPO-*p*, TFPPO, TClPPO, and TBrPPO) in ethyl acetate (5 mg $mL^{-1}$) were added into the solution with a volume ratio of 1:2 during the second-round purification process. For QLED device optimisation, we have shown the performance of typical QLEDs with different concentrations of TMeOPPO-*p* in ethyl acetate (**Fig. R3.15**).

In FTIR results, the C-H stretching modes (2700~3000 $cm^{-1}$) from OAm/OA ligands were weakened in target QDs (**Fig. R3.16a**), indicating that TMeOPPO-*p* could partially connect with the uncoordinated $Pb^{2+}$ and replace the ligands. In NMR results, the $^{1}H$ NMR spectra of the target QDs showed a higher chemical shift, while the $^{31}P$ NMR spectra of the target QDs showed a lower chemical shift (**Fig. R3.16b, c**). The P=O bond in TMeOPPO-*p* coordinated with $Pb^{2+}$ in the form of a double bond. This process not only formed a sigma coordination bond but also allowed the d orbitals of the Pb atom to interact with the π*-antibonding orbital of the double bond, creating a π backbonding. This delocalised the charge on the Pb and increased the π-electron density, thereby slightly shifting the $^{31}P$ NMR peak upfield. In contrast, when the methoxy group

bound to Pb, no π backbonding was formed, resulting in a reduction of the electron cloud density around the hydrogen atoms and a downfield shift in the $^{1}$H NMR peak. In sum, the FTIR and NMR results indicated that TMeOPPO-*p* could partially replace the ligands, thus avoiding the weak and dynamic connection between ligands and QDs.

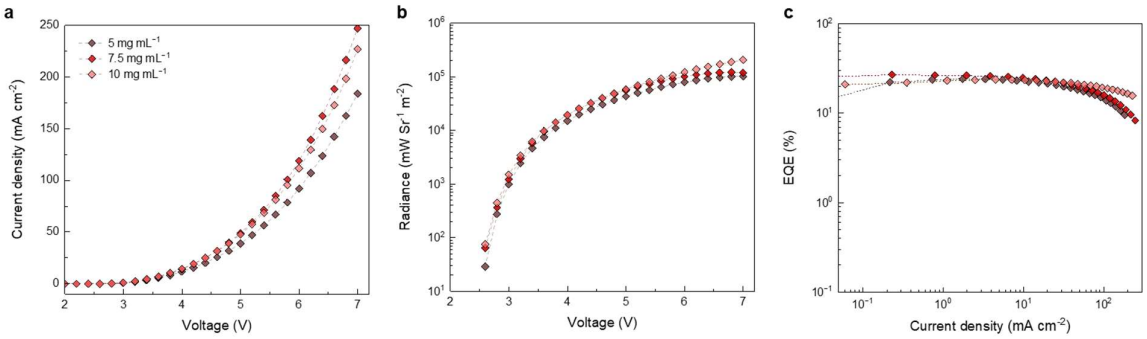


**Fig. R3.15** Performance of target QLEDs with different concentrations of TMeOPPO-*p* in ethyl acetate. **a**, 5 mg mL$^{-1}$. **b**, 7.5 mg mL$^{-1}$. **c**, 10 mg mL$^{-1}$. (**Fig. S7** in revised Supporting Information)

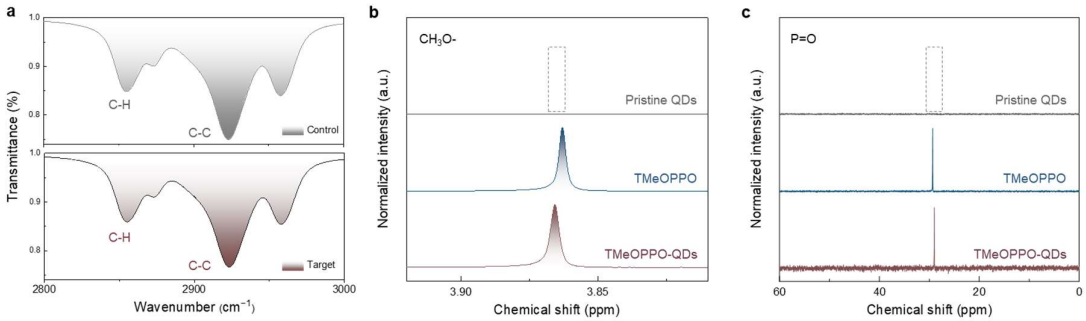


**Fig. R3.16 a**, FTIR spectra of the QDs. **b**, $^{1}$H NMR spectra of the pristine QDs, TMeOPPO-*p*, and target QDs. **c**, $^{31}$P NMR spectra of the pristine QDs, TMeOPPO-*p*, and target QDs.

ii. The description of sample fabrication and characterisation processes lacks important details. For instance, with regards to HTL, the authors simply wrote "a mixture of PEDOT: PSS and PFI solutions was spincoated onto ITO-coated glass substrates" without mentioning the concentration and choice of solvents; For air-processed QLEDs, the authors wrote "we spun PEDOT:PSS:PEI, PTAA and QD solution in the atmosphere" without mentioning important details such as humidity; For PL measurement, the excitation source, its wavelength and fluence are not mentioned.

**Response:** To ensure the reproducibility of the experimental results, our laboratory has been maintained at a

temperature of approximately 25°C and a relative humidity of 20-30%. We have now included more detailed information on the specific ambient humidity and sample during the preparation of the perovskite layer for each entry.

We have now added the corresponding contents as follows:

**Page 8**: Notably, the $^{1}$H NMR spectra of the target QDs showed a higher chemical shift, while the $^{31}$P NMR spectra of the target QDs showed a lower chemical shift. The P=O bond in TMeOPPO-*p* coordinated with $Pb^{2+}$ in the form of a double bond. This process not only formed a sigma coordination bond but also allowed the d orbitals of the Pb atom to interact with the π*-antibonding orbital of the double bond, creating a π backbonding. This delocalised the charge on the Pb and increased the π-electron density, thereby slightly shifting the $^{31}$P NMR peak upfield. In contrast, when the methoxy group bound to Pb, no π backbonding was formed, resulting in a reduction of the electron cloud density around the hydrogen atoms and a downfield shift in the $^{1}$H NMR peak.

**Page 12**: The maximal EQE of the target QLED reached 26.91% with optimised concentrations of TMeOPPO-*p* in ethyl acetate (**Fig. S7)**, achieving a considerable improvement compared to the control device (**Fig. 4f**).

**Page 4** in Supporting Information: For treated QDs, different molecules (TPPO, TMeOPPO-*o*, TMeOPPO-*p*, TFPPO, TClPPO, and TBrPPO) in ethyl acetate (5 mg $mL^{-1}$) were added into the solution with a volume ratio of 1:2 during the second-round purification process.

**Page 7** in Supporting Information: For the hole transport layer, a mixture of PEDOT: PSS (Baytron P VPAl 4083) and PFI solutions (filtered through a 0.22 μm filter) at a mass ratio of 1:1 were spin-coated onto the ITO-coated glass substrates at 4000 r.p.m. for 45 s, followed by annealing at 150 ℃ for 30 min in the atmosphere.

**Page 7** in Supporting Information: For air-processed QLEDs, we spun PEDOT: PSS: PFI, PTAA and QD solution in the atmosphere at approximately 25°C and a relative humidity of 20~30%.

**Page 8** in Supporting Information: PL spectra were obtained by using a Varian Cary Eclipse spectrometer (F-7000 FL Spectrophotometer; Excitation light source: xenon lamp; Excitation light wavelength: 405 nm; Scan speed: 240 nm/min).